Novel Nuclear Magnetic Resonance Coil

For Magnetic Resonance Mesoscopy

by

Haiqing Wang

A Thesis Presented in Partial Fulfillment
of the Requirements for the Degree
Master of Science

Approved November 2014 by the
Graduate Supervisory Committee

Vikram Kodibagkar, Chair
Sarah Stabenfeldt
Rosalind Sadleir

ARIZONA STATE UNIVERSITY

December 2014

ABSTRACT

Magnetic Resonance Imaging (MRI) is an efficient non-invasive imaging tool widely used in medical field to produce high quality images. The MRI signal is detected with specifically developed radio frequency (RF) systems or "coils". There are several key parameters to evaluate the performance of RF coils: signal-to-noise ratio (SNR), homogeneity, quality factor (Q factor), sensitivity, etc. The choice of coil size and configuration depends on the object to be imaged. While surface coils have better sensitivity, volume coils are often employed to image a larger region of interest (ROI) as they display better spatial homogeneity.

For the cell labeling and imaging studies using the newly developed siloxane based nanoemulsions as ^{1}H MR reporter probes, the first step is to determine the sensitivity of signal detection under controlled conditions in vitro. In this thesis, a novel designed 7 Tesla RF volume coil was designed and tested for detection of small quantities of siloxane probe as well as for imaging of labeled tumor spheroid. The procedure contains PCB circuit design, RF probe design, test and subsequent modification. In this report, both theory and design methodology will be discussed.

ACKNOWLEGEMENTS

First of all, I would like to express my deep and sincere appreciation to all of people who have ever helped me during these two years.

Thanks my parents, for giving me life, financially and emotionally supporting my study. I would not exist without you. Words cannot express my gratitude and will not be able to.

I am grateful to my mentor Professor Vikram Kodibagkar. It was he who led me to explore this unique and promising Biomedical Engineering field - Magnetic Resonance Imaging. I knew him through his MRI class and it was the most difficult course for me, but I found it interesting and start to get more interested in it. After that semester, I requested this thesis topic from him and started to work in ProBE lab. As a mentor, Professor Vikram Kodibagkar always had an open door and willing to answer any questions. As a leader, he is able to keep us cooperating closely so that our lab was on the path to becoming experts in MRI field. He encourages students to research independently and cares about the comprehensive answers to the research. Our weekly lab meeting provides us a great opportunity to report progress, discuss questions and plan next steps. I would not have able to finish this thesis without his help and encouragement. I will miss this period of time working here. Professor's courses, advice, insights, help, even coffee were extremely valuable to my work. He has provided me with experience in a new research platform and resources: preclinical MRI devices, circuit designing and cell culture, and for all that, I am forever grateful.

Many thanks to Professor Sarah Stabenfeldt and Professor Rosalind Sadleir. They approved me to use their facilities and I would also like to thank them for being my committee members.

Special thanks to my ProBE lab members, they have been giving me biggest motivation and inspiration in this past two years.

Alex Cusick was a responsible researcher and had a fine sense of humor. He kept us working in an easy and positive atmosphere. He taught me fundamental lab training and the manufacture of nanoemulsion, cell culture and labeling. I am proud of being a peer with him look forward to watching his achievement in his interested field.

Shubhangi Agarwal was always there whenever I had any question or needed some help. She had helped me a lot in my experiment and drove me to the lab in Phoenix many times. Her motivation and passion for science is truly admiring. She is a good peer and friend. I am sure she will do an extraordinary work in future.

Rohini Vidya Shankar was the first person taught me how to run the MRI system and process the following data. She was always ready to help others whenever any question came. She was learned, consistently hard-working and rigorous. I have no doubt she will make a significant achievement in this field.

I would like to thank to all researchers in Barrow Neural Institute Preclinical Imaging Lab, especially Qingwei Liu. They had helped me a a lot in my experiment and helped train me to run the Bruker MRI system.

Finally, I would like to thank anyone who has supported me over the past two years again, my family, all professors, classmates, friends and research faculties.

Research is never easy, and so many people were there to pick me up every time I fell. The sacrifice of your time was an incredible blessing in my life.

I will leave someday, but my research never stops. I had never regretted working here and will be always proud of that.

TABLE OF CONTENTS

Page

CHAPTER Page

Page

LIST OF FIGURES

Figure Page

Figure Page

1 INTRODUCTION

1.1 Problem Statement

The RF (Radio Frequency) coils are one of the most important components of the whole Magnetic Resonance Imaging system with function of transmitting and receiving high frequency electromagnetic signals to reconstruct an image of biological entity. Generally, they can be classified into two types: RF surface coils and RF volume coils. Surface coils exhibit a good sensitivity but they cover a small area so that their field of view is small. Also, the homogeneity of surface coils is not as good as volume coil, which means the localization will be crucial because adjusting position of coil or the position of sample is not feasible while imaging. On the other hand, volume coils have excellent homogeneity so that are able to produce uniform magnetic field in imaging region but require that the sample be entirely contained in the coil.

The goal of my research is to image the siloxane resonance from tumor spheroid cells labeled with siloxane nanoprobes. The challenge here is imaging a tiny volume of spheroid sample (600-800 um) with high sensitivity and homogeneity at same time. The main challenge is the extremely low sample volume, due to which, the intensity of NMR signal will be so weak that is hard to detect by current coil. Previous efforts in our lab to image labeled spheroids using a commercial Bruker coil were unsuccessful. Thus, there is a need to design and test a specific RF coil system for spheroid imaging.

1.2 Objectives

The objective of my research here is to design and test an RF suitable for imaging mesoscopic scale objects (100-1000 μm) and employ it for imaging spheroids labelled with siloxane nanoprobes at 7 Tesla using a Bruker MRI system. Approach here is to design the specific schematic of the coil circuit, followed by the performance testing, analyze and compare my coil with commercial RF coil and demonstrate the feasibility of application.

2 NMR PRINCIPLES

Magnetic Resonance Imaging is an efficient non-invasive imaging tool widely used in medical field to produce high quality images. It has gained this widely reputation due to its outstanding sensitivity and flexibility to a wide range of tissue properties [1]. Comparing with other common imaging techniques like X-ray and CT (computed tomography), MRI is much safer because no exposure to ionizing radiation is needed. Also the rapidly increasing applications of MRI and improvement in imaging acquisition continue to further enhance MRI.

2.1 Nuclear Magnetic Resonance

The fundamental operational mechanism of MRI is nuclear magnetic resonance phenomena. Nuclear magnetic resonance is closely related with nuclear spin: it occurs when the nuclei of atoms are immersed in a static magnetic field first and another oscillating magnetic field applied to it. The main principle of nuclear magnetic resonance comes from quantum mechanical interaction between magnetic field surrounding and atomic nuclei inside [1]. As an analogy, we can use classical physics to describe its interactions.

2.2 Magnetic Spin

The spin is a fundamental physical property of nature like mass and charge. Protons, neutrons and electrons all possess this natural property. The nuclei of ^{1}H (quite abundant in biological tissues and biochemicals) has only one proton, and we can consider its interaction under magnetic field.

The classical theory regard the proton as a tiny sphere with uniformly positive charge distributed. The proton has its mass and can be considered as a rotating charge in this classical analogy (Fig 1). This rotation generates the angular momentum and then, current produced from this motion of charge. At last, the current loop generates magnetic field.

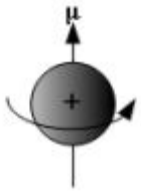

Fig 1. **Magnetic Spin.** Spinning charge of proton produces nuclear magnetic moment **μ**

The relationship is given [1]:

$$\boldsymbol{\mu}=\gamma * \mathbf{J} \qquad (2.1)$$

μ: magnetic moment

γ: gyromagnetic ratio, 267.5MHz/T when it is hydrogen proton

J: angular moment

Once the situation of two or more proton exist, the angular momentum of each proton will be assumed in opposite direction, up and down only, to avoid creating degeneracy. So, only odd number of protons will generate angular momentum and we call that net nuclear spin.

2.3 Effect of Magnetic Field

There are two energy state of nuclei spin when a static magnetic field employed: lower one and higher one. The energy difference between these 2 state is proportional to the intensity of magnetic field. This is called Zeeman effect. When it reach the thermal equilibrium, the number of nuclei in higher energy state is slightly less than that in lower state. A photon with same energy as the difference gap between higher and lower state will be generated and emitted out, when the proton fall down from higher state to lower state, or vise versa, absorb energy and jump from lower to higher state. Diagram is shown below (Fig 2).

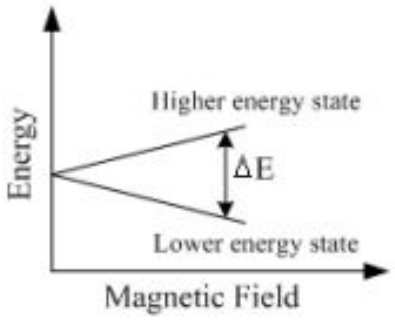

Fig 2. **Splitting of Energy State** [2]

2.4 Magnetization Process

Firstly, a strong uniform magnetic field $\mathbf{B_0}$ is applied externally . Therefore, the individual magnetic moments will align themselves along this outer magnetic field $\mathbf{B_0}$. Once these magnetic moments starts to align with the magnetic field $\mathbf{B_0}$, it is known that a parallel state or a antiparallel state if against the magnetic field.

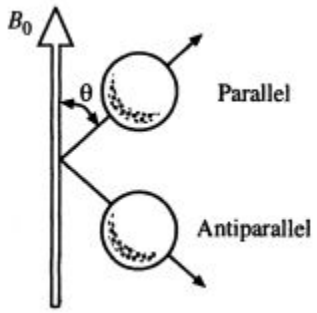

Fig 3. **Nuclear Magnetic Moments Aligned in The Direction of External Magnetic Field** [2].

The nuclei are randomly oriented when in a none magnetic field and total value is zero magnetic moment from looking outside. However, when a magnetic field is employed on it, individual moment will be re-distributed by external magnetic field. Single nuclei will start to align with external magnetic field $\mathbf{B_0}$ and this process produces magnetization along $\mathbf{B_0}$ direction. The higher energy spins align along the direction of the external magnetic field and outnumber the lower energy spins creating a net magnetization known as M_0.

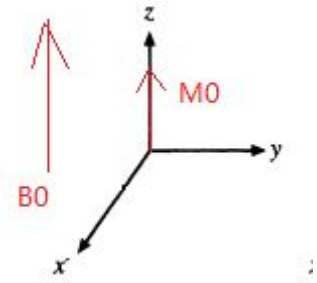

Fig 4. **Magnetic Field M_0 Along External Magnetic Field** B_0.

Then an electromagnetic wave (usually RF pulse) is employed and the its precessional axis is shifted away from the axis of the uniform magnetic field $\mathbf{B_0}$ and starts precessing. The frequency of magnetization M_0 is precessing around $\mathbf{B_0}$ at is known as Larmor frequency. Larmor frequency is dependent on static field strength and governed by the following equation :

$$\omega = \gamma \mathbf{B_0} \qquad (2.2)$$

where $\mathbf{B_0}$ is the magnetic field strength (Tesla), γ is the gyromagnetic ratio (nuclei dependent) and ω is the Larmor frequency.

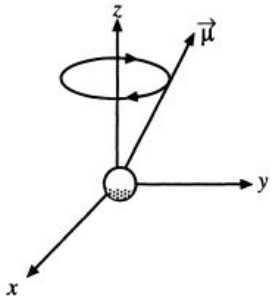

Fig 5. **Magnetic Moment Vector Processing About the Axis of Static B_0 Magnetic Field** [2].

Resonance is achieved when the frequency of the RF pulse of strength $\mathbf{B_1}$ matches Larmor frequency. The flip angle determines the amount of magnetization flipped into the transverse plane:

$$\Theta = \gamma \int_0^{T_p} B_1 \, dt \qquad (2.3)$$

The time during which the B_1 field is employed determines the flip angle, and when turned off, the nuclear spins return to align along the static magnetic field B_0. The process is known as relaxation and occurs as a longitudinal T1 and transverse T2 component.

The time constant which describes how the magnetization returns to equilibrium along the longitudinal Z axis is known as T1. Following equation is used to describe the relationship between M_0 and relaxation vector Mz:

$$M_z = M_0 (1 - e^{-t/T1}) \qquad (2.4)$$

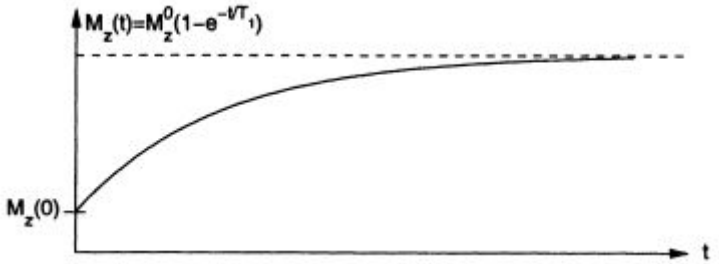

Fig 6. **T_1 Relaxation Curve.** Longitudinal magnetization tends to grow with time constant T_1 [2].

The time constant which describes how the magnetization returns to equilibrium in the XY-plane is known as T_2 time. Following equation is used to describe the relationship between M_0 and transverse vector M_{xy}

$$M_{xy} = M_0 (e^{-t/T2}) \qquad (2.5)$$

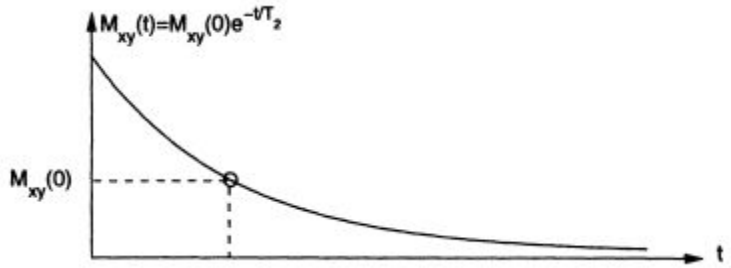

Fig 7. **T_2 relaxation Curve.** Transverse magnetization tends to decay with time constant T_2 [2].

However, relaxation time T1 and T2 are not the only factors affects the image intensity. There are many approaches of getting an MRI image and detailed discussion is beyond the scope of this thesis. The basic principle I will show here is a radio frequency signal is induced in a receiving coil that is laid perpendicular B_0 field. This signal from coil will be received in conjunction with applied gradient fields, processed and eventually transformed into image.

2.5 MRI Hardware

The MRI system is a sophisticated instrument, with various . It consists of several functional components that need to operate synchronously as per the instructions in the user selected "pulse sequence" . Figure 8 shows a general MRI system structure.

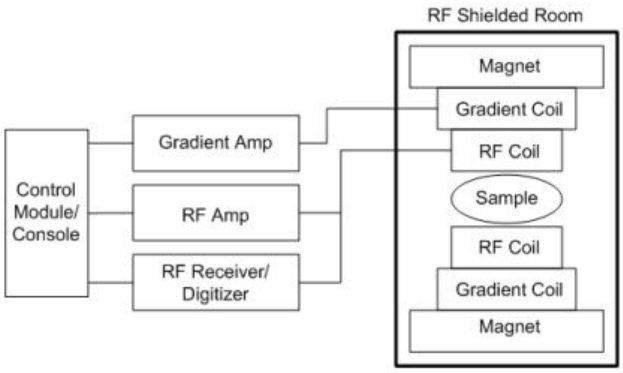

Fig 8. **MRI Block Diagram** [1].

2.5.1 Magnet

The role of magnet is generating strong background magnetic field B_0 which is uniform in the volume of imaging area. The intensity of magnetic field generated needs to be strong to provide a better signal-to noise ratio and resolution, both in frequency and spatial domains. According FDA regulations, the clinical MRI magnets up to 3 Tesla are approved for routine human use. Preclinical scanners often use magnets of 7-9.4 Tesla or more.

2.5.2 Transmitting and Receiving Coil

RF coils create the B_1 field which rotates the net magnetization according to the pulse sequence [3]. They also detect the transverse magnetization as it precesses in the XY plane. RF coils can be divided into three general categories; 1) transmit and receive coils, 2) receive only coils, and 3) transmit only coils. Transmit and receive coils serve as the transmitter of the B_1 fields and receiver of RF energy from the imaged object. A transmit only coil is used to create the B_1 field and a receive only coil is used in conjunction with it to detect or receive the signal from the spins in the imaged object. The design, testing and application of a receiving coil is the subject of my thesis.

2.5.3 Gradient Coil

Gradient coil encodes the nuclear spins spatially by generating a position-depended varying magnetic field and causes the Larmor precessional frequency to depend on and hence encode position [1]. Typically, it applies field gradients along three physical axes: X,Y, and Z gradient and the dependence of field on location is linear (i.e. first order gradients are used).

3 NANOEMULSION SILOXANE PROPERTIES

3.1 Chemical Shift

When the transverse non-equilibrium nuclear spin magnetization is precessing about the Z-axis, a current will be generated in a coil around the X-axis. The signal produced by plotting this current as a function of time and this signal is called Free Induction Decay (FID). This signal can be converted into the frequency domain by a fourier transform and resultant spectrum can aid in siloxane selectivity via the chemical shift phenomenon.

The chemical shift comes from inherent differences in the resonance frequency of precessing protons [4]. The phenomenon is caused by variations in electron density due to differences in types of nuclei and molecular bonding [4]. In other words, the information in FID reflects the status of excited protons and the actual number of that depends on the chemical structure and bonding of the ^{1}H atom to other atoms. The chemical shift of a specific nucleus is measured as the difference between its resonance frequency and a standard. This property is measured in ppm and given the symbol δ [5].

$$\delta = [(\nu - \nu_{ref}) * 10^{6}]/ \nu_{ref} \qquad (3.1)$$

For instance, water and fat are most common ^{1}H containing chemicals in animals or cells. We can identify their relative concentrations by using this chemical shift. This information is used to create an NMR spectra using tetramethylsilane as standard (0 ppm)

relative to which water appears at 4.7 ppm, fat falls at 1.0 ppm, and siloxane falls between -0.5 and 0.5.

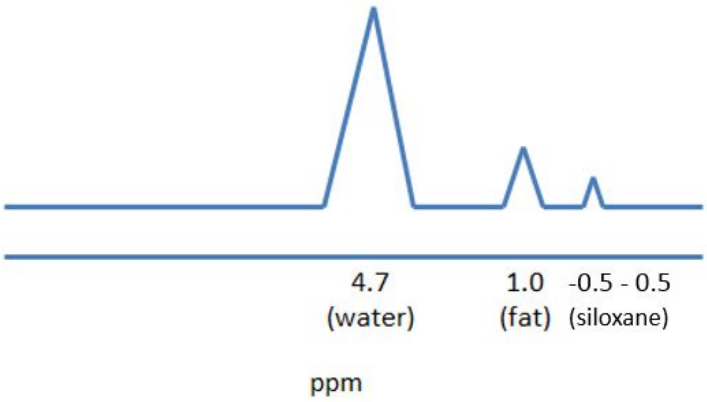

Figure 9. **Example NMR Spectra**. Each hydrogen-containing molecule resonates at a specific frequency with respect to a standard.

The nanoprobes used for cell labeling are able to generate signal that is well separated in frequency from the background ^{1}H (mostly from water or fat in imaging human tissue) signal due to chemical shift [6]. Proton imaging of siloxane to map tissue oxygenation levels (PISTOL) employs a chemical-shift selective (CHESS) spin echo sequence to locate hexamethyldisiloxane (HMDSO) [7]. This sequence provides optional water and fat suppression along with a long echo time (>50 ms) for additional fat suppression [7]. T_1 mapping can quantify pO_2 and provide functional oximetry essential for cell labelling applications.

3.2 Fluorescence

The second property of siloxane-based nanoprobes is fluorescence. A fluorophore is a fluorescent chemical compound capable of absorbing energy and re-emitting light of a specific wavelength upon light excitation [8,9]. Each fluorophore has an excitation and emission spectra.

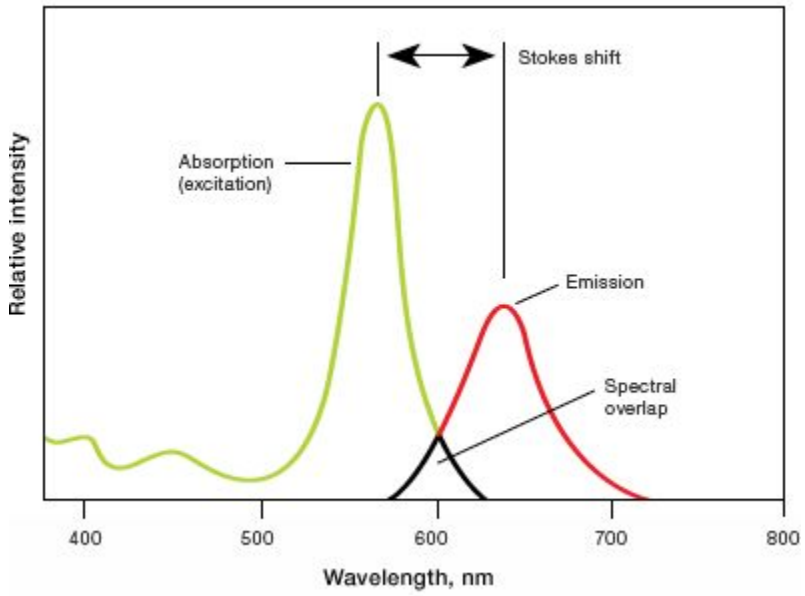

Fig 10. **Excitation/Emission Spectra of Undefined Fluorophore.** The excitation bandwidth (peak near 560 nm) and emission bandwidth (peak near 650 nm) allow for light detection of a specific fluorophore (from http://www.bio-rad.com/en-us/applications-technologies/detection-methods).

4 PARAMETERS OF COIL

4.1 Signal to Noise Ratio

In MRI system, the desired signal from the sample of interest is always contaminated by noise from random fluctuating currents in coil and the sample itself [10]. Therefore, the signal to noise ratio (SNR) is an important factor to evaluate a coil. However, SNR in MRI system depends on a number of factors: the type and structure of coil, imaging parameters such as resolution and bandwidth, etc.

The SNR is generically described as [3] :

$$SNR \propto \frac{V_s w^2 B_1}{f_n \sqrt{4kTr\Delta f}} \qquad (4.1)$$

Where we have, V_s is the volume of phantom, the Larmor frequency w, magnetic field intensity B_1, K is Boltzmann's constant, T is temperature, r is resistance, f_n is noise factor. And bandwidth of freq Δf. In given phantom and outer experimental environment, the resistance r is the only factor I can control.

In MRI imaging field, the signal-to-noise ratio is used as a physical measure of the sensitivity of imaging system. Generally, SNR in imaging field is defined:

$$SNR = \frac{\mu_{sig}}{\sigma_{noise}} \qquad (4.2)$$

In this case, SNR is the ratio of the average signal value μ_{sig} to the standard deviation of the noise σ_{noise}.

Industry standards measure and define sensitivity in terms of SNR: 32.04dB=excellent image quality and 20dB=acceptable image quality [11].

4.2 Quality Factor

Another important parameter of circuit is quality factor Q. It is measure of return loss of a circuit, and is affected by factors like the strength of B_1 magnetic field, SNR, sensitivity etc. The Q is defined in terms of the ratio of the energy stored in the resonator to the energy supplied by a generator, per cycle, to keep signal amplitude constant, at resonant frequency.

$$Q = 2\pi \times \frac{\text{Energy Stored}}{\text{Energy dissipated per cycle}} \quad (4.3)$$

For high values of Q, the following definition is also mathematically accurate:

$$Q = \frac{f_r}{\Delta f} = \frac{w_r}{\Delta w} \quad (4.4)$$

Where f_r is the resonant frequency, Δf is the half power bandwidth. W_r is the angular resonant frequency, and Δw is the angular half power bandwidth. These values can be measured from a plot graph of energy versus frequency.

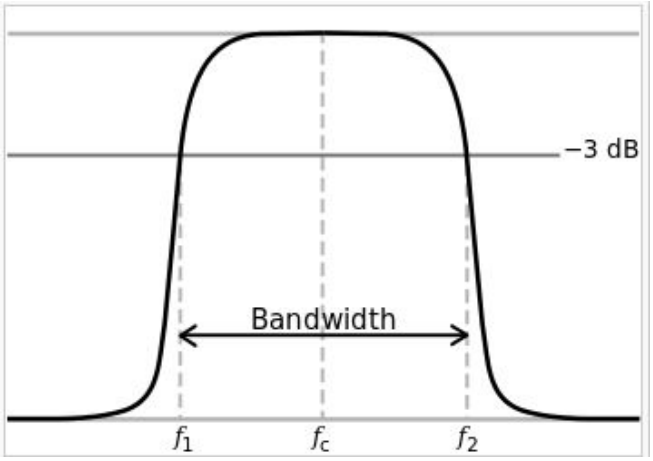

Fig 11, **Energy to Frequency Curve**, the bandwidth of a damped oscillator is shown. The Q factor is $f_c/\Delta f$. The higher the Q, the narrower and sharper the peak is.

In my research, the Q factor can be measured directly by VIA ECHO MRI (0.1T to 20T) MRI/NMR Network Analyzer (AEA Technology. Inc)

4.3 Sensitivity and Filling Factor

Sensitivity is defined as how weak signals the coils can detect. The higher sensitivity coil has, the lower signals we can detect. However, the higher volume of undesired noise we will obtain as increasing sensitivity and that will lower the SNR. Ultimate sensitivity format is given in time domain as followed [3]:

$$S = \frac{2B_1}{I_0} N_0 \frac{\gamma^3 \hbar^2 s(s+1)}{3k_B T} B^2 (\sin\theta) \delta V_e \frac{1}{\sqrt{4rk_B T \delta f}}. \qquad (4.5)$$

Under the certain circumstance of given sample, the nuclear species γ, spin s , and the number of nuclei N_0 will be fixed. For given observation using a given scanner, B, θ,

§V_e and §f is fixed. Thus we can simplify this equation and the sensitivity is proportional to B_1, current I and resistance r. Furthermore, if the RF field generated is uniformly distributed in coil, sensitivity can be replaced by square root of filling factor times Q. The filling factor indicates the ratio of sample volume to the inner volume of coil. So increase filling factor also favors sensitivity.

4.4 Homogeneity

In this research, homogeneity It means the magnetic field must be very homogeneous over the observed volume of the sample. Because in this scenario, all of the spins within the observation volume have the same magnetic field. A lack of homogeneity means that the various spins experience different magnetic fields.

The electromagnetic wave decreases dispreads as the distance increase. Thus the magnetic field B1 produced by RF coils is not homogeneity. Inhomogeneity could be caused by the geometric shape of coil, the magnet design, materials in the probe, variations in the thickness of the sample tube, sample permeability, and ferromagnetic materials around the magnet. All factors affect the image quality directly.

4.5 Tuning and Matching

In general, a resonant circuit can be tuned to the frequency of the corresponding nucleus and matched to the standard impedance of the connecting lines, usually 50 ohm. This is usually achieved by adjusting variable capacitors in the circuit. Tuning and

matching reduces reflected power and increase the quality factor Q, leading to shorter pulse widths and better sensitivity but also to stronger radiation damping in presence of strong signals.

Tuning is necessary when using different samples with the same probe circuit. This is due to sample's RF properties. Its dielectric constant affects the probe tuning by adding a capacitance. The sample's conductivity results in "loading" the circuit, the effect is similar to placing a resistor across the coil, i.e. the circuit impedance is affected. So, if the probe is not properly tuned, RF power is not optimally transferred, thus worsening SNR.

Matching circuit is an important part in RF circuits. When the circuit is connected to a source or loaded, the load impedance will differ from the source impedance leading to reduction in output. The matching network is required to deliver maximum power from source to the load. The condition is given by the conjugate matching theorem which states that maximum power is transferred if and only if the impedance of the signal source is equal to the load impedance.

4.6 Choice of Coils

We have discussed these several key factors of coil so far, however we can not build a perfect coil that works for every application. Designing RF coils, requires a compromise between generating a uniform magnetic field and getting a good signal-to-noise ratio. A large coil own wide field of view and more uniform magnetic field. However, the smaller coil has better SNR than larger one. Consequently, RF circuit has to consider the size of coil and object are taken. There are numerous types of RF coils that have been developed and they are generally classified into two groups: volume coils and surface coils. Examples of these two are shown in figure.

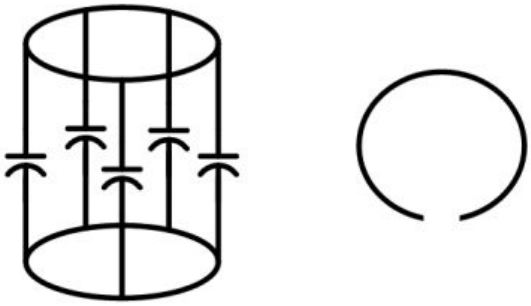

Fig 12. **Classic Bird Cage Volume Coil And Circular Loop Surface Coil**

A volume coil is used to generate a uniform magnetic field over a larger area. The sample is always enclosed by coil. High homogeneity is another advantage of volume coil because the distance from coil elements to sample to be imaged is uniform on average.

Surface coils can be single loop or multi-loop coils. Their shapes are uncertain,

can be round , rectangular or splay. But the common point is they need to be place over the region of interest. Since they are smaller than volume coils, they sacrifice uniformity for higher SNR. That is also my decision: A high SNR, small FOV, receiving surface coil.

5 DESIGN AND CONSTRUCTION OF AN RF COIL FOR MESOSCOPIC SCALE APPLICATION

5.1 Design And Model

Typically, a surface coil is constructed using conducting wires or copper tape as inductor and ceramic chip capacitors. There are several analytic and numerical approaches to model surface coils. Each method has different capabilities with different degree of accuracy. The series-wound circuit model is one of traditional methods of modeling coil [1] and is shown below. And basic principle of this model is connecting all inductive and capacitive accessories in series. In this case, the coil is treated as a lumped inductor and likewise, capacitive element is treated as lumped capacitor. This model is mostly used for MRI RF coil modeling and my design is also based on this model.

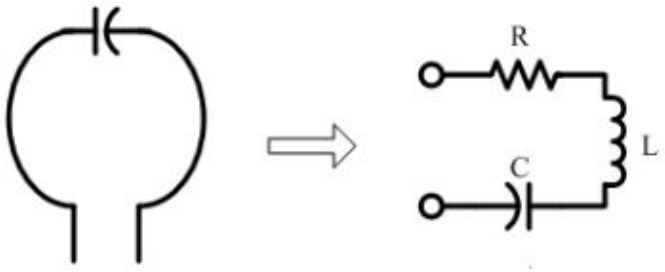

Fig 13. **Equivalent Model of Line Coil**

Most RF coils are designed based on the concept of resonance. Coils are composed of capacitive and inductive accessories. These elements determine the center

resonance frequency of coil. The relation between frequency, value of inductor and capacitor is given:

$$F = \frac{1}{2\pi\sqrt{Lc}} \tag{5.1}$$

Where, F is center frequency which used in actual experiment. In my research, it is 300MHz. L is the number of inductor and c is that of capacitor.

As I discussed in chapter 4.3, the main function circuit part in RF circuit can be separated into working coil, tuning circuit and matching circuit. OrCAD Pspice 9.1 student version (available from http://www.electronics-lab.com/) was used to design the circuit. OrCAD is a useful tool to design and simulate analog and digital circuits. The circuit design is shown in Figure 14.

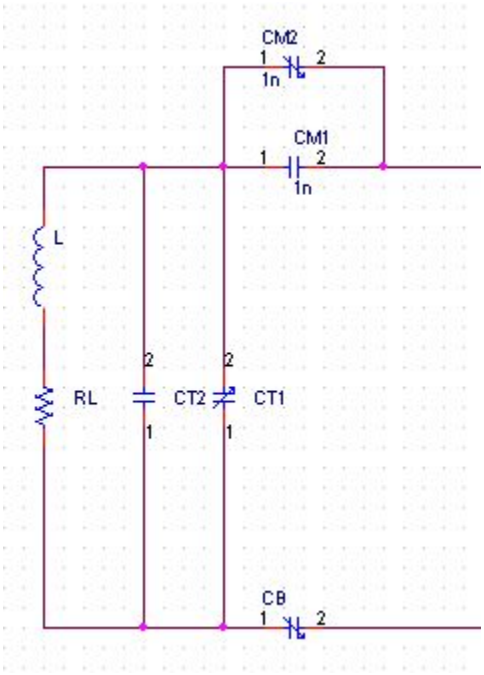

Fig 14. **Schematic of RF Circuit**

The value of all accessories are not labeled here because the inductance of coil is uncertain. The inductance of coil is determined by its shape and physical properties and I will discussed it later.

5.1.1 Symmetrical Capacitive Coupling

The necessity to use a balanced matching network has been well demonstrated for in vivo experiment [12] and widely accepted in almost all NMR probe design, especially those dealing with animal or human experiment.

The idea is very simple and consists of splitting the fixed matching capacitor of the standard circuit in two capacitors both ends of the coil, one to the ground and the other one to the cable central connection (Fig 15)

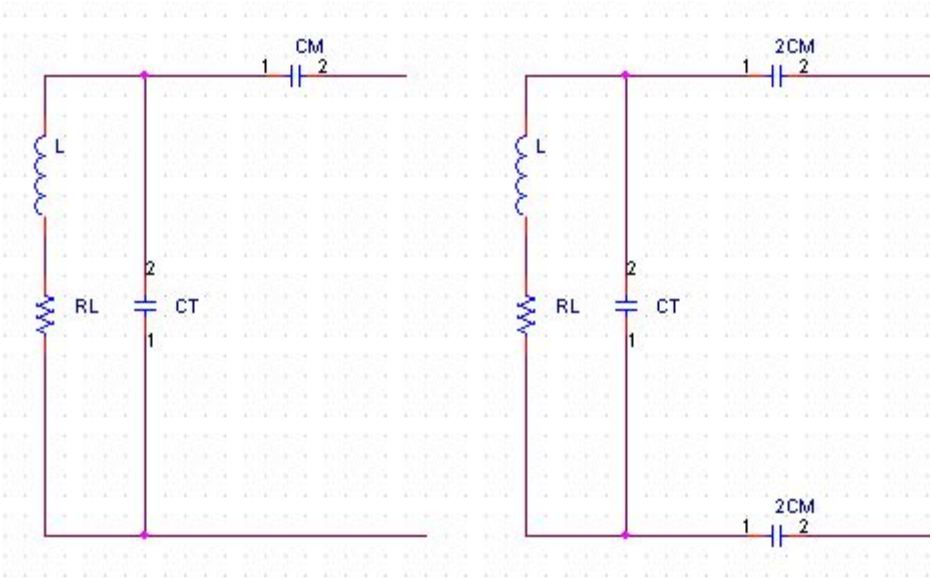

Fig 15. **Conversion of Basic Circuit**, capacitive matching circuit (left) into a balanced matching circuit (right)

The same current flows through both capacitors and because they have same impedance, the voltage with respect to ground at the two coil ends is almost equal and of opposed phase, realizing the required electrical balancing. Furthermore, the voltage amplitude is halved as compared to the unsymmetrical case, providing the expected reduction in electrical loss. The virtual ground point is located near the center of the coil, also resulting in a reduction in radiation losses due to the antenna effect. Ideally, the voltages would be exactly of opposed phase and of the same amplitude. However, in fact, the symmetry is only approximate due to the resistance of coil. As a result, the voltages exhibit, small, in phase, real component and large, out of phase, imaginary components. I wrote a Matlab code to simulate the phase plot of voltage in figure 15 and details are provided in appendix.

5.1.2 Components Chart

A list that shows each component's function is in figure 16.

Name	Function
VinAC	Simulate the function of receiving coil, generating AC current signal
RL	Coil's self resistance
L	Coil's inductance
CT1, CT2	Tuning fix and adjustable capacitors
CM1, CM2	Matching fix and adjustable capacitors

Fig 16. **Coil Components**, list of all potential components in circuit

Once the geometric design is determined, the next step is to design the dimension of coil inductor and measure the inductance and resistance of the same.

5.2 Calculation

In order to determine the value matching and tuning capacitors, we first, simplify initial design (Fig 14) into the following circuit:

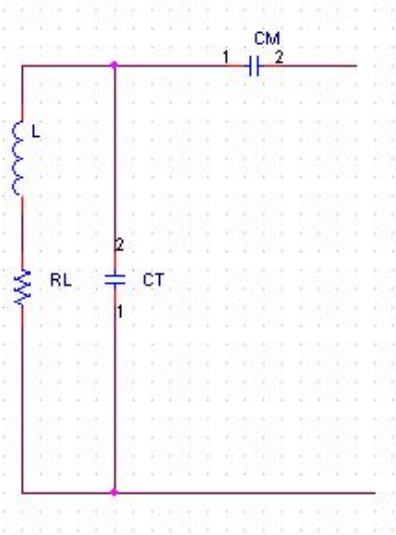

Fig 17. **Simplified Schematic**

Quantitatively, the impedance Z of parallel circuit above is given by:

$$\frac{1}{Z_{parallel}} = \frac{1}{R + jwL} + jwC_T \tag{5.2}$$

After solving for $Z_{parallel}$ we get

$$Z_{parallel} = \frac{R \cdot (\frac{1}{c_T{}^2 w^2})}{R^2 + (wL - \frac{1}{c_T w})^2} - \frac{j}{c_T w} \cdot \frac{R^2 + w^2 L^2 - \frac{L}{c_T}}{R^2 + (wL - \frac{1}{c_T w})^2} \tag{5.3}$$

Thus, total impedance Z_{total} is:

$$Z_{total} = \frac{R \cdot (\frac{1}{c_T{}^2 w^2})}{R^2 + (wL - \frac{1}{c_T w})^2} - j(\frac{1}{c_T w} \cdot \frac{R^2 + w^2 L^2 - \frac{L}{c_T}}{R^2 + (wL - \frac{1}{c_T w})^2} - \frac{1}{w c_m}) \tag{5.4}$$

The resonant frequency of probe should be first adjusted so that the real part of Z should be equal to 50 ohms at the spectrometer frequency f=300Mhz. This is done by adjusting the tuning capacitor C_T as followed

$$Z_{real} = \frac{R \cdot (\frac{1}{c_T{}^2 w^2})}{R^2 + (wL - \frac{1}{c_T w})^2} = 50\Omega \tag{5.5}$$

Solving above equation, obtain:

$$C_T = \frac{\frac{Lw}{R} \pm \sqrt{\frac{R + \frac{L^2 w^2}{R}}{50} - 1}}{wR + \frac{L^2 w^3}{R}} \tag{5.6}$$

The reactive component of Z_{total} is obtained by

$$Z_{image} = -50 R c_m w (1 + \frac{w^2 L^2}{R^2} - \frac{L}{R^2 c_m}) \tag{5.7}$$

From above equations and after some algebraic manipulation, one obtains the reactive component of the probe resonator at center frequency f:

$$Z_{image} = \mp 50\sqrt{\frac{R + \frac{w^2 L^2}{R}}{50} - 1} \tag{5.8}$$

The plus sign in the equation above corresponds to the minus sign in equation 5.6. In this case, the reactive impedance is inductive and will be compensated by matching capacitor C_m as follow:

$$c_m = \frac{1}{50 \cdot w\sqrt{\frac{R + \frac{w^2 L^2}{R}}{50} - 1}} \tag{5.9}$$

If, the plus sign is chosen in equation 5.6, the matching component must be an inductor L_m

$$L_m = \frac{50\sqrt{\frac{R + \frac{w^2 L^2}{R}}{50} - 1}}{w} \tag{5.10}$$

This configuration is often referred to as the series matched/ parallel tuned circuit. In my experiment, the surface coil designed to work at 300MHz so angular speed $w=2\pi*3X10^8$ rad/s. The coil has an inductance of 13nH and resistance 0.2 ohm. I then used Matlab to calculate the values of each component, the code is attached as appendix in bottom. The tuning capacitor is 23.0061pF and the Matching capacitor has to be 1.3808pF. This leads to a theoretical quality factor Q=122.52 .

5.3 Construction

5.3.1 PCB Manufacture

Photo lithography based etching was used to make PCB board. First, the circuit path was designed using SolidWorks and printed on a common transparency. As this probe operates at 300MHz, two parallel copper path may influence each other and cooperate as a capacitor. Therefore, two-sided circuit design was discarded to minimize the occurrence of parallel circuit path. Parallel gaps were reserved for capacitors and inductors.

Next, the copper clad board (MG chemicals, Ontario, Canada) and transparency were cut into appropriate size. Figure 18 is the photo of ready to use transparency:

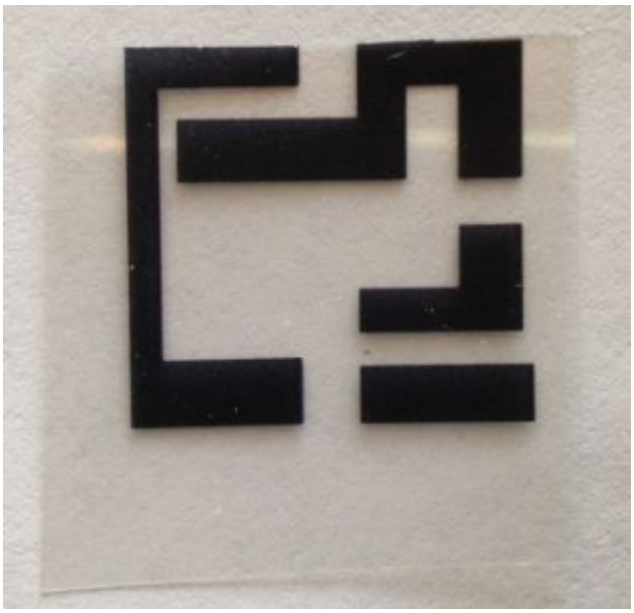

Fig 18. **Printed Transparency**. Note: the ink is easily scratched so have to handle it carefully.

The plastic layer covering copper clad board was peeled in darkness (as it is sensitive to light), the transparency was attached on it using tape to bind them tightly. This was important as many bubbles can be left behind between the transparency layer and board if it wasn't tight enough. Furthermore, these bubbles will scatter the UV light and worsen the performance of lithography.

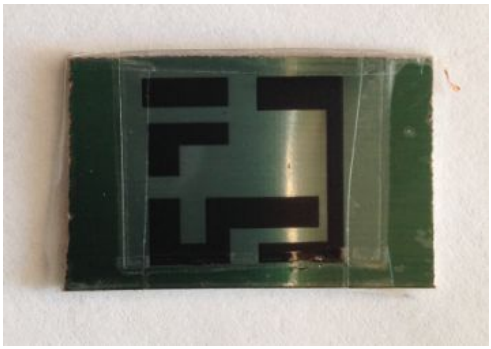

Fig 19. **Tightly Bound Transparency and Board.** Make sure bindings are tight and no visible air bubble in it.

The board was exposed to ultraviolet light by UVGL-25 Compact UV lamp (UVP, Upland, CA, USA) for 15 minutes. 254nm short wave settings were selected.

Fig 20. **Configuration of UV Light Box.** Surrounding walls are black to minimize UV scattering.

While the exposure was running, 5ml positive type developer concentrate (GC Electronics, Rockford,USA) was mixed with 45ml water to get positive developer solution, transferred solution into a small tray for use. The etching solution was transferred into small glass beaker and diluted.

After the UV exposure the board was taken out and immersed into positive developer solution after removing the transparency. The developer solution was agitated by BioRocker (Denville Scientific Inc) at 80 rpm speed. This procedure proceeds quickly so the board needs to be monitored constantly. The board needs to be removed from solution as soon the circuit paths were clearly seen because the paths will be etched if the reaction is allowed to proceed.

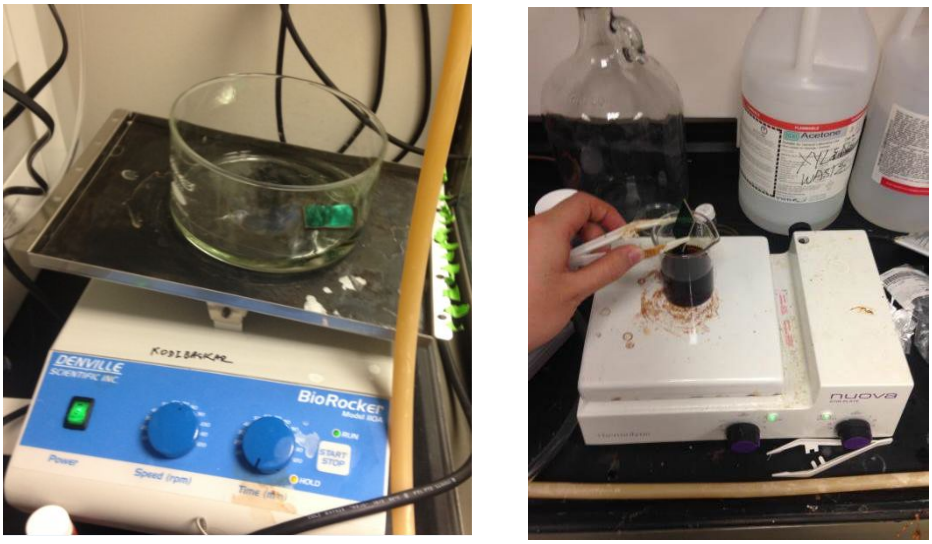

Fig 21. **Circuit Board Developing (left) and Etching (right)**

The board was then rinsed and then immersed into PC Board Etching Solution under stirring at 60 centigrade (Hotplate and Stirrer, Denville Scientific Inc). After 10 minutes, the circuit paths were clearly seen with green color and all background copper

was seen to be etched. The board was then removed and rinsed with water followed by acetone.

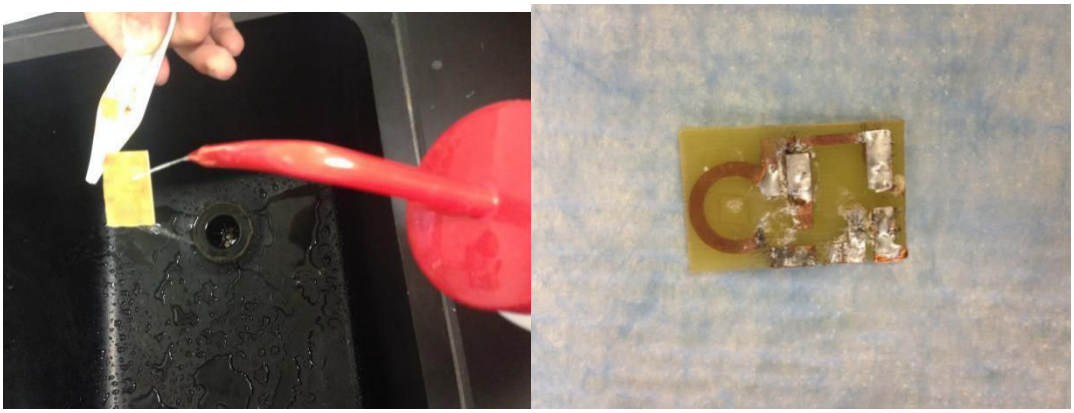

Fig 22. **Flushing and Trail Board**

5.3.2 Coil Manufacture

A 3D printer was used to build skeleton of coil with following parameters: 10mm height; 4.5mm inner radius; 5.5mm outer radius. These number corresponded to the smallest size of tube we had. Thus, my coil covers container tightly and achieved the best fill factor for maximum sensitivity. A copper foil was taped on the on outer surface of the skeleton and this served as the inductor for the circuit.

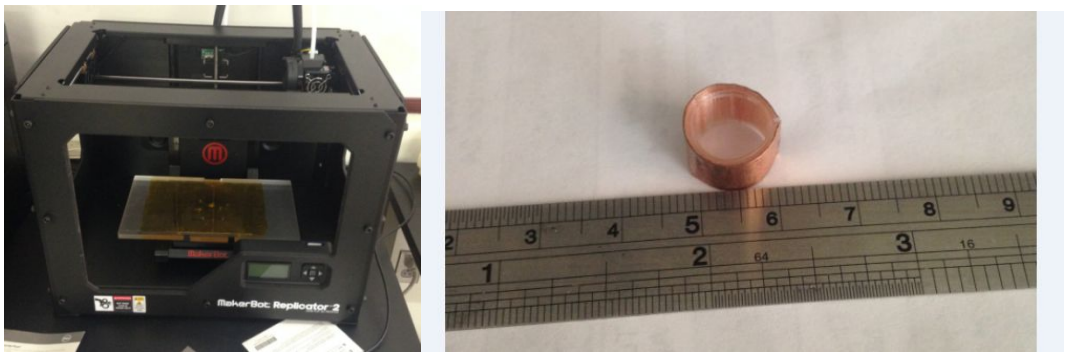

Fig 23. **3D Printing Coil and Finished Product**

5.3.3 Assembling and Testing

All accessories were soldered on the PCB to complete the coil construction. The coil is shown in figure below. For details of components, see appendix.

Fig 24. **Overview of All Accessories and Soldered Product**

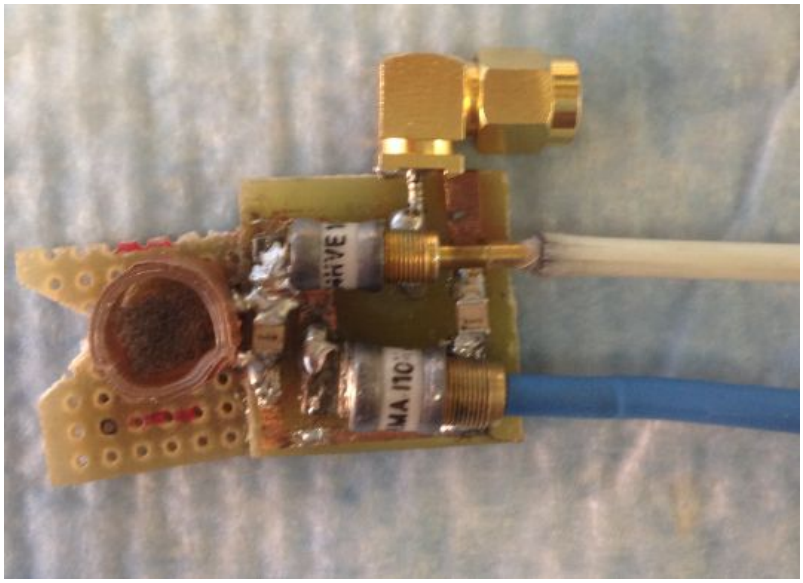

Fig 25. **Top View of Coil**

The coil was then tested for resonance at 300 MHz using a VIA ECHO MRI 0.1T to 20T MRI/NMR Network Analyzer (AEA Technology. Inc) and the Q factor was measured as shown in Figure 27.

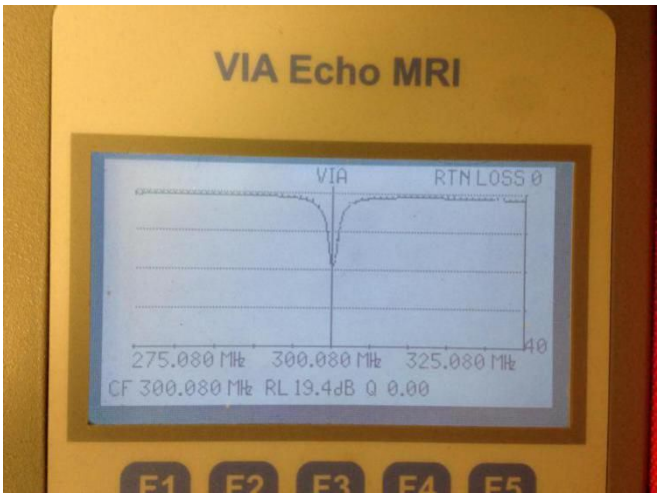

Fig 26. **Q Factor Measurement**

6 COIL PERFORMANCE TESTING AND APPLICATION TO SPHROID IMAGING

6.1 Tumor Spheroid Culture

[Special thanks to Alex Cusick and Shubhangi Agarwal for providing details.]

Human prostate carcinoma epithelial cells, 22Rv1 (ATCC; Manassas, Virginia, USA), were used for cancer cell labeling studies. Mouse embryonic fibroblast cell line, NIH/3T3 (ATCC) was used for conjunction incubated with 22Rv1 cells for tumor spheroid formation.

22Rv1 were plated on T75 cell culture flasks (Fisher Scientific; Hampton, New Hampshire) and cultured in Rosewell Park Memorial Insititue (RPMI) media (ATCC). Once the cells reached 80-95% confluency at a 10 µL/mL concentration, continue incubation for 1-3 hours. After that, the media/nanoparticle mix was removed and the cells were washed with 3 mL of Dulbecco`s Phosphate Buffered Saline (Thermo Scientific; Waltham, Massachusetts) for 2-3 minutes. DPBS was removed and cells were trypsinized using 5 mL of Trypsin 0.25% (1X) solution (Thermo Scientific). At this point, the cells lost adherence to the flask surface, were removed, spun down, re-suspended and ready for experimental use.

In a 100mL Pyrex media bottle, a 1% agarose (Sigma-Aldrich; St. Louis, Missouri) gel solution was prepared using non-supplemented Dublecco's Modified Eagle's Medium (DMEM). This mixture was autoclaved, and 50µL of solution was placed in each well of a 96-well plate before solidifying. While pipetting, care was taken

to ensure no bubble formation in the agarose gel. The 96-well plate was covered from light and allowed to cool for 1.5 hours.

NIH/3T3 and 22Rv1 cells were cultured alongside agarose plating. The two cell lines were mixed in a 1:1 ratio in an equal amount of DMEM and RPMI to a cell concentration of 600,000 cells/mL (final seeding density 120,000 cells/well). 200 μL aliquots were pipetted into each agarose-coated well and incubated. RPMI/DMEM mixture was added every 24-48 hours depending on nutrient uptake. Spheroids were ready for experimental use after 72 hours.

6.2 Nanoemulsion Preparation and Labeling

[Special thanks to Alex Cusick for providing details]

Nanoprobe synthesis was performed at 70°C and particle composition was as follows, 55% deionized water, 40% siloxane, and 5% surfactant (emulsifying agent). Deionized water was attained from Arizona State University laboratory facilities. PDMS (Alfa Aesar, Ward Hill, Massachusetts, USA) with a molecular weight of 410 g/mol was utilized in place of siloxane. Solutol® HS 15, received as a gift from the BASF Corporation (Florham Park, New Jersey,USA), was used as the emulsifying agent. Fluorophores Nile Red was used in emulsion synthesis.

Initially, HS 15 was heated and transitioned from a solid to liquid state within a 20mL scintillation vial (Sigma-Aldrich; St. Louis, Missouri, USA). Deionized water was measured out accordingly and placed in a vial. This vial was placed on a heat/stir plate

within a water bath. After the system reached 70°C, as measured by a temperature probe, HS 15 (in liquid state) was added to deionized water.

While mixing occurred, PDMS and a fluorophore were combined via following methodologies. For Nile Red (Fisher Scientific; Waltham, Massachusetts, USA), ethanol was used to dissolve Nile Red at a ratio of 3.9 mg/mL. Once dissolved, Nile Red/ethanol was added to PDMS at a volume resulting in 0.1mM final Nile Red dye concentration in the emulsion. The dye was added on a heat/stir plate for 5 minutes at 70°C in an effort to force ethanol evaporation.

The PDMS/fluorophore combination was added to the deionized water/surfactant mixture in a drop-by-drop fashion to allow for particle formation. The mixture was allowed to sit at 70°C for 15 minutes prior to sonication. Sonication occurred for a total of 45 minutes (3, 15 minute intervals) at 150W and a duty cycle of 50%, using an Omniruptor 4000 Ultrasonic Homogenizer (Omni International; Tulsa, Oklahoma, USA). The sample was de-bubbled and filtered with CELLTREAT (Celltreat Scientific; Shirly, Massachusetts, USA) 0.22μm syringe filters 10 times prior to particle size measurement. Nanoparticles were characterized using Delsa Nano Particle Size Analyzer (Beckman Coulter; Pasadena, CA, USA) through Dynamic Light Scattering (DLS).

Particle size typically ranged from 50nm – 150nm following sonication and filtration. Peak number average of diameter of particle, which used in section 6.6, was within an average to be 120.24 ± 18.3 nm.

Following spheroid formation, nanoemulsion was added to the DMEM/RPMI mixture at a concentration of 10 μL/mL and placed in the spheroid-containing wells. After an hour of incubation, the nanoemulsion/media solution was removed from the well.

Spheroids were washed three times with PBS and placed in new wells containing nanoemulsion free media.

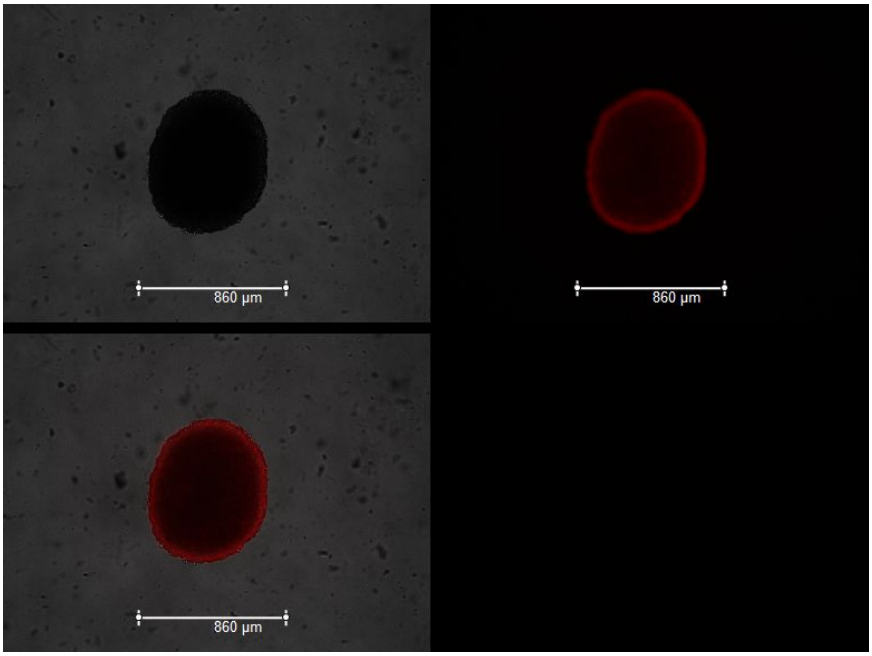

Fig 27**. Tumor Spheroids Labeled with Nanoemulsion After Structural Formation.** **(A)** Bright Field image **(B)** Fluorescence image **(C)** Overlay. Scale bar is 200 microns.

6.3 Coil Characterization

All imaging studies took place on the Pre-clinical Bruker (Billerica, MA, USA) 7T magnet at Barrow Neurological Institute/Arizona State University facilities within St. Joseph's Hospital (Phoenix, AZ).

First, a series of tests were performed to gauge the coil performance and compare with commercial coil to qualify this novel coil. The setup for these tests are given in table below

Phantom	1. 50ul Agarose, . 2. 50ul Agarose+10ulPDMS
Pulse Sequence	RARE T1, MSME T2
Matrix Dimension	64*64
Recovery Time (TR)	3000ms for T2 mapping
Echo Time (TE)	11ms for T1 mapping
Field of View (FOV)	2cm (axial),1cm(coronal)
Slice Thickness	0.5mm
Average Number	1
NEX	1
RF Pulse	Sinc7H, sinc3
Angle	90/ 180

The only differences between each imaging experiment for comparing my coil with the Bruker coil are location and number of slices. It is impossible to ensure exactly same location when I switch the samples but the relative position was calculated and I ensured that sampling areas are close. Secondly, the hieght of sample is latger than diameter so more slices needed, which extend the TR time between axial and coronal T2 imaging.

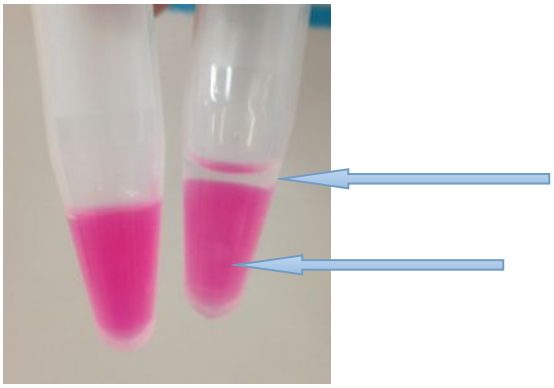

Fig 28. **Agar Sample and Agar/PDMS Dual Layer Sample.** Arrows show transparent PDMS. The droplet in the center of the vial on the right is hard to see.

6.3.1 SNR Evaluation

SNR (signal to noise ratio) and CNR (contrast to noise ratio) were used as criterion to evaluate the performance of coils. Red symbols indicate the performance of my designed coil and the green one comes from the Bruker mouse head coil.

SNR=mean intensity of ROI / (Std Dev of background noise).

Contrast to noise ratio, $CNR=SNR_a-SNR_b$

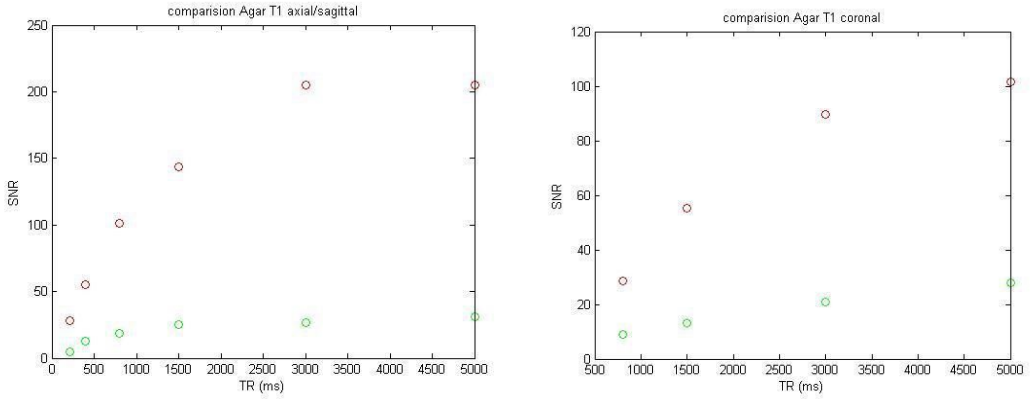

Fig 29. **Agar Sample, SNR Curve for T1 Mapping in Axial and Coronal Direction**.

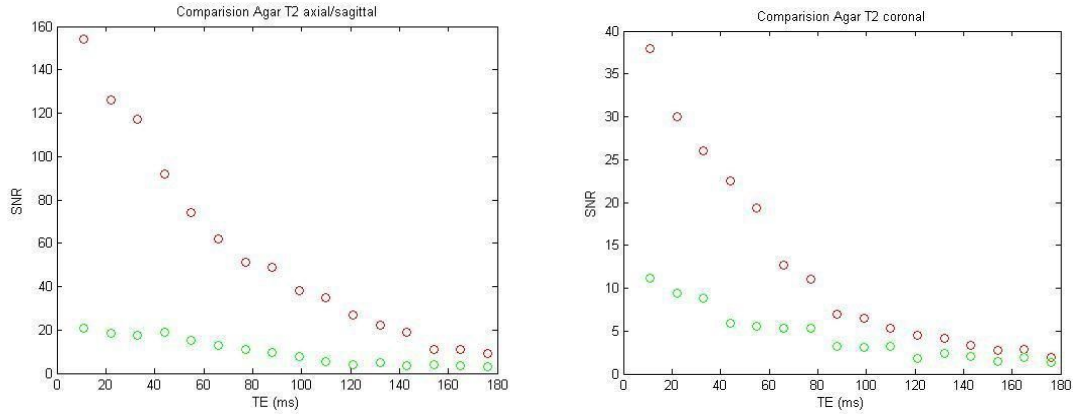

Fig 30. **Agar Sample, SNR Curve for T2 Mapping in Axial and Coronal Direction.**

The results above show this new coil provide about four or five times increase in SNR for agar sample. For contrast to noise ratio (CNR), we need to measure both SNR of agar and PDMS.

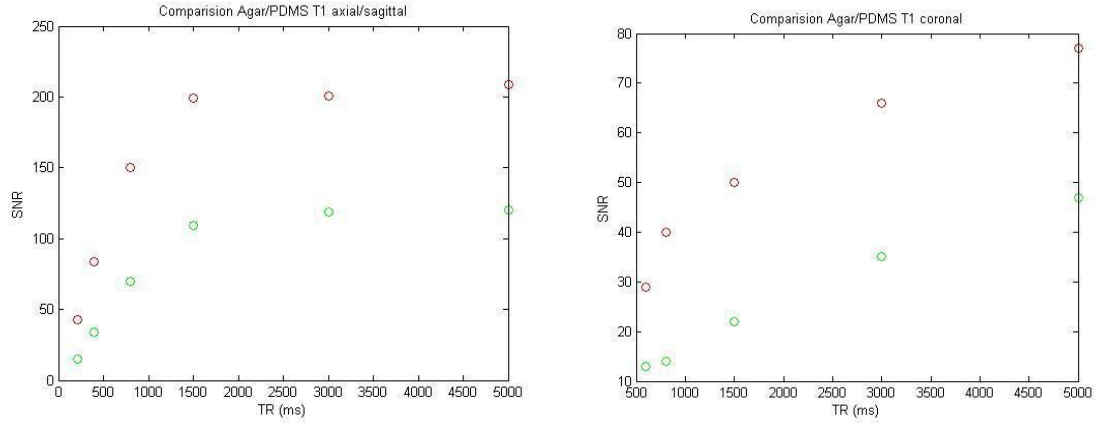

Fig 31. **Agar/PDMS Sample, SNR Curve for T1 Mapping in Axial and Coronal Direction.**

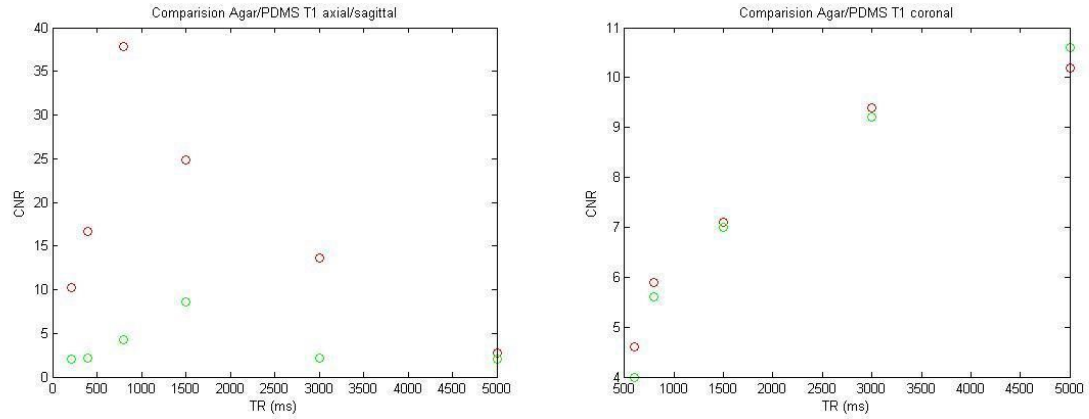

Fig 32. **Agar/PDMS Sample, CNR Curve for T1 Mapping in Axial and Coronal Direction.**

The results above show this new coil provide an good increase in SNR and CNR for Agar/PDMS subject. However, the CNR in coronal T1 for new coil remains the same level with commercial coil and I will discuss this later.

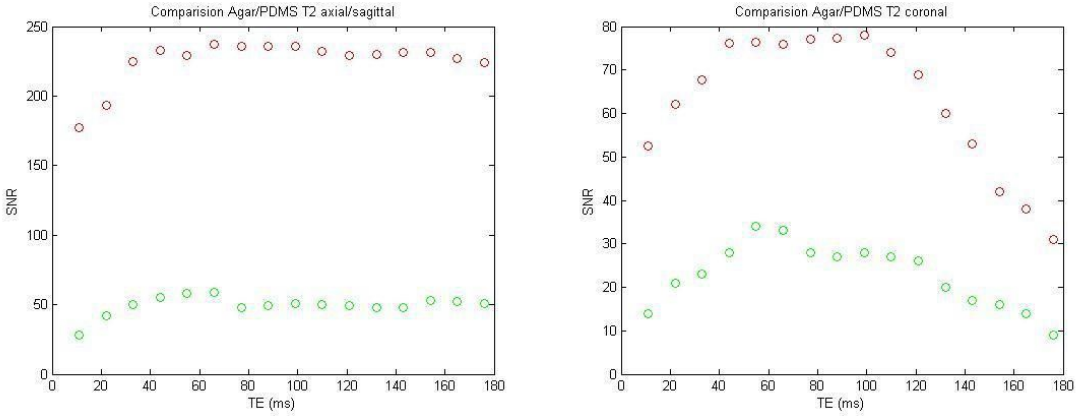

Fig 33. **Agar/PDMS Sample, SNR Curve for T2 Mapping in Axial and Coronal Direction.**

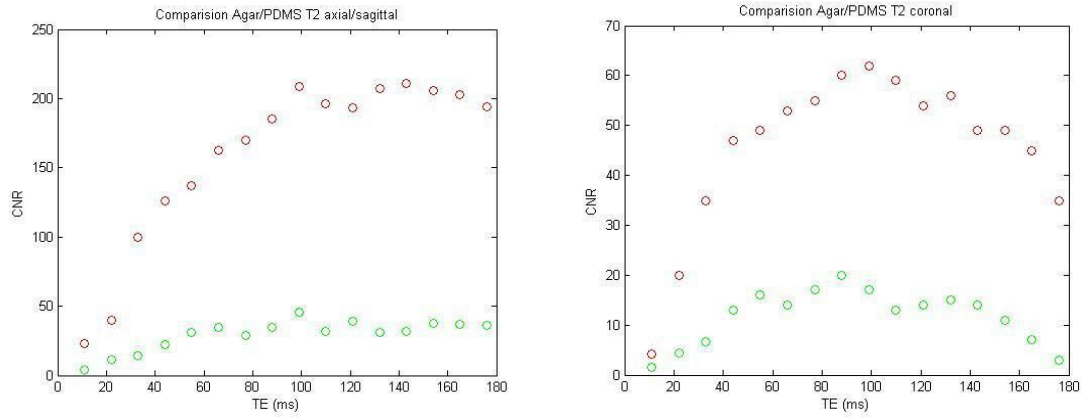

Fig 34. **Agar/PDMS Sample, CNR Curve for T2 Mapping in Axial and Coronal Direction.**

These results show that the new coil performed much better than commercial Bruker mice head coil and hence was used to perform subsequent studies.

6.3.2 Homogeneity Evaluation

Besides SNR and CNR characterization, homogeneity of the coils were compared as well. The agar sample was chosen and T2 weighted imaging was performed with TR=3000ms and TE=110ms. At short TE values, points in image appeared saturated in intensity and long TE images had lower SNR as expected. Thus a middle TE value was picked for the homogeneity analysis. Using Matlab to convert image data into matrix, a line intensity profile was measured at column or row. Red lines in the following images

indicate the sampling location. Both Bruker and my coil were compared using axial and coronal slices.

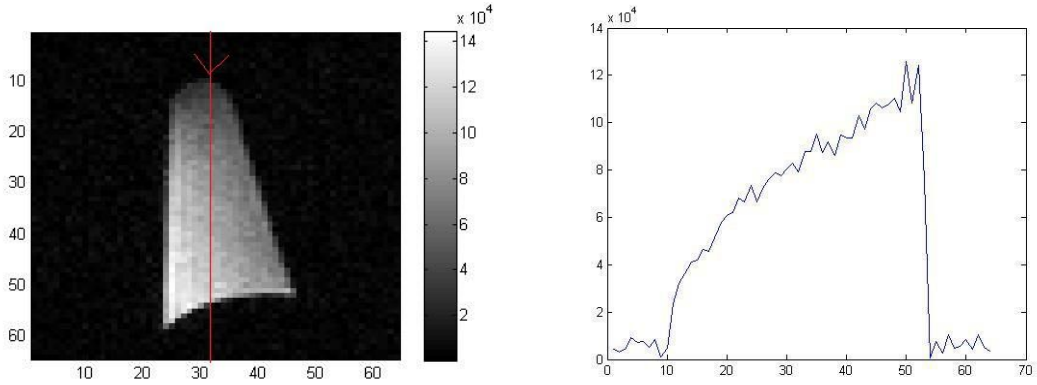

Fig 35. **Homogeneity of Bruker Coil along Axial Direction.**

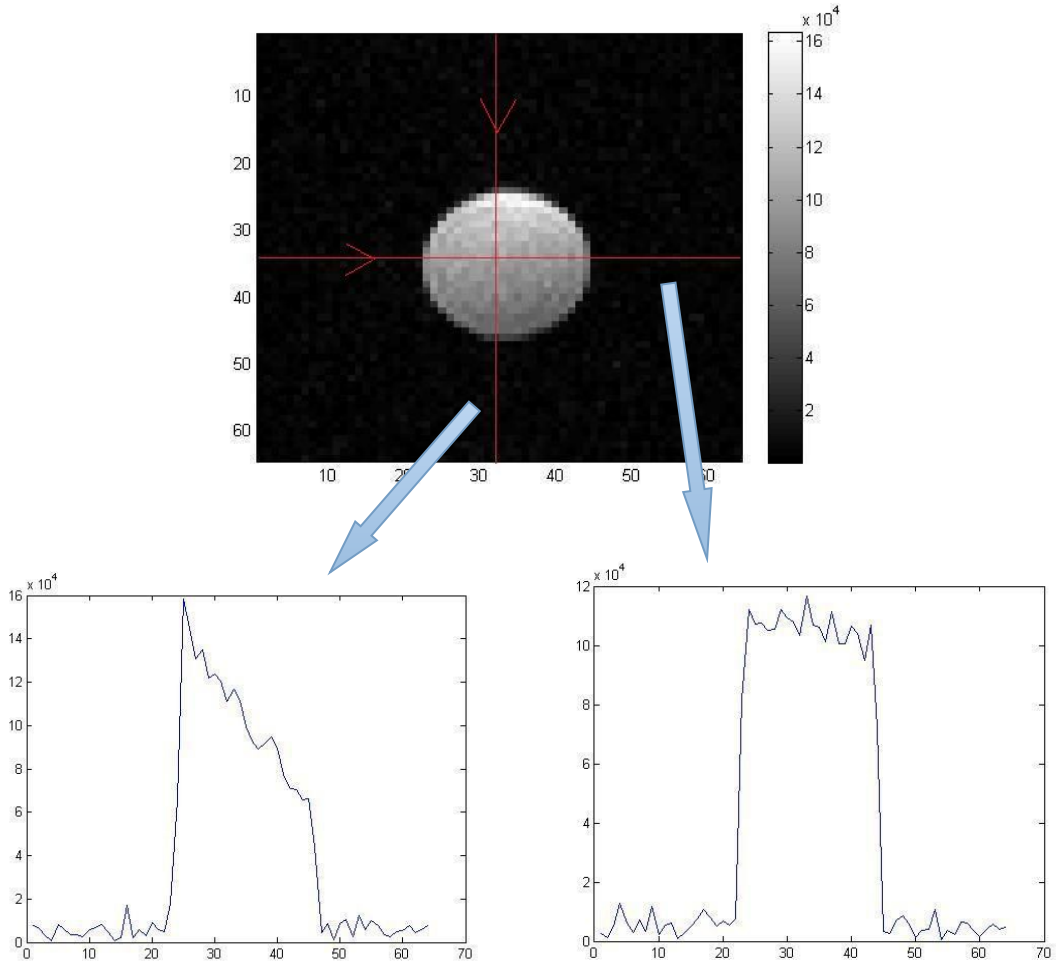

Fig 36. **Homogeneity of Bruker Coil along Coronal Direction.**

One point we cannot ignore is the differences in the FOV of coils being compared. The Bruker coil is large to cover the whole sample but my coil was designed for mesoscopy, which means the upper part of Agar exceeded the 10mm length of the coil. In subsequent spheroid experiments we do not need to image that region either.

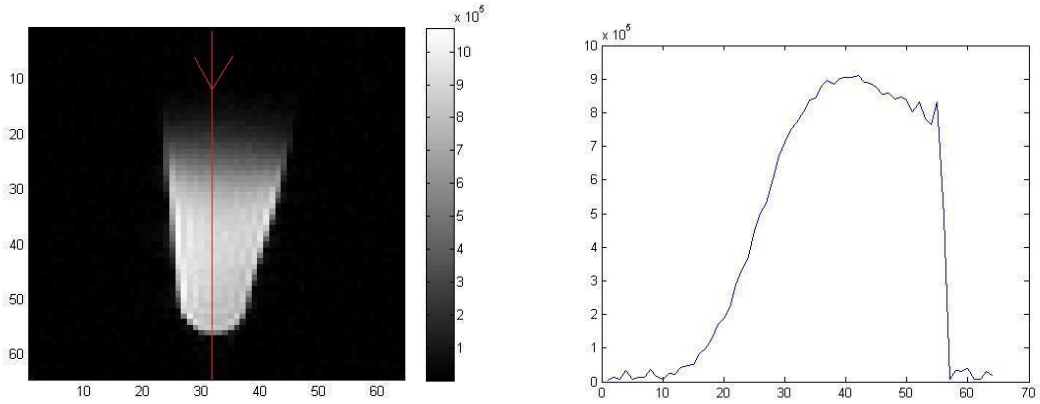

Fig 37. **Homogeneity of Designed Coil along Axial Direction.**

The whole volume of coil covered starts from clear seen bottom to the geometric position corresponding to 35th pixel here. Therefore it shows a sharp edge and uniform middle part if we consider the region physically covered by coil.

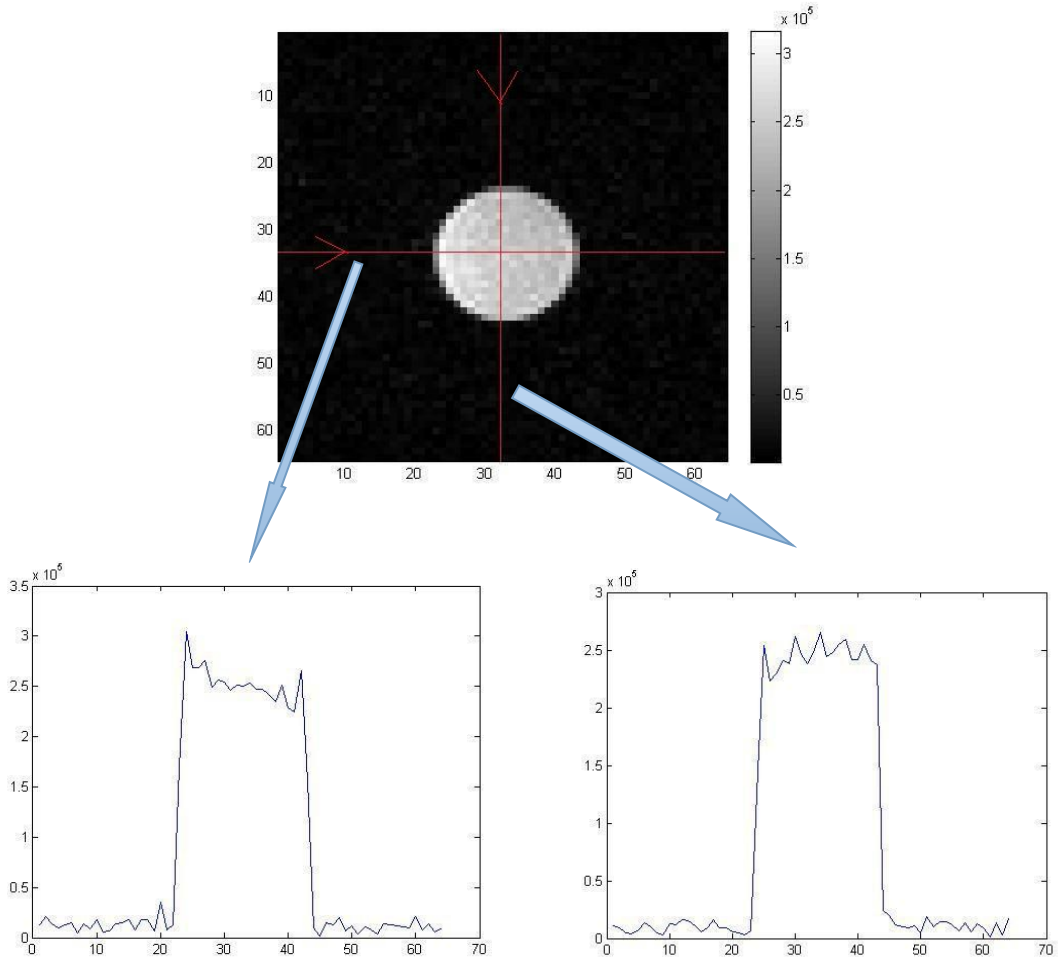

Fig 38. **Homogeneity of Designed Coil along Coronal Direction.**

In conclusion, new loop gap coil and appropriate filling factor favors homogeneity and sensitivity as well. Next characterization is quality factor which will give us an evaluation of coil efficiency.

6.3.3 Q Factor Evaluation

As discussed before, the quality factor 'Q' is defined in terms of the ratio of the energy stored in the resonator to the energy supplied by a generator, per cycle, to make

the output signal Q times of input, at resonant frequency. It favors the SNR and sensitivity directly and determines the efficiency of total system. The performance of Bruker coil and designed coil were compared after tuning and matched to center working frequency 300MHz.

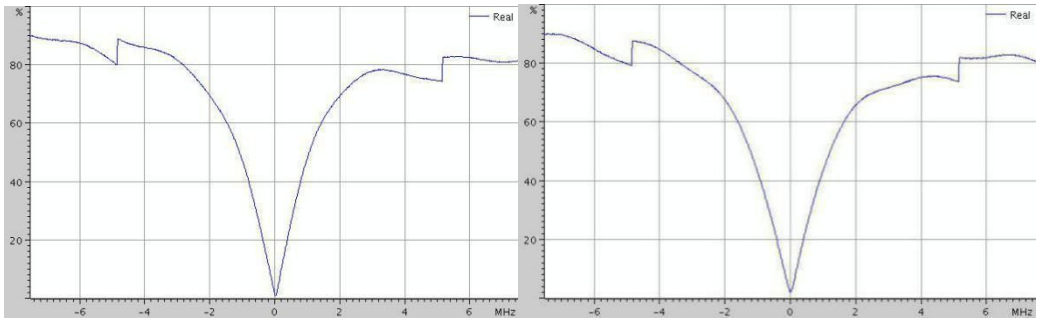

Fig 39. **Q Curve of Bruker Coil and Designed Coil.**

Measured out the half-power points in Bruker's coil are ±1.1386 at 50.4% and (1.0149/50.13%). Corresponding points for my coil are ± 1.1376/50.13%. Applying the formula in section 4.2 and we obtain a Q of 140 in the Bruker coil and 132 in my coil. However, my coil will have a better performance and sensitivity in the situation of almost same quality factor because of the optimal fill factor.

6.4 T2 Imaging of Tumor Spheroid

Since new coil showed improved performance over the commercial coil, the next trial was to detect the unlabeled spheroid tumor cells. Experimental parameters are:

Phantom	Tumor spheroid cells
Pulse Sequence	RARE T1, MSME T2
Matrix Dimension	64*64
Recovery Time (TR)	T1:600ms, T2:3000ms
Echo Time (TE)	T1:9ms, T2:60ms
Field of View (FOV)	2cm (axial),1cm(coronal)
Slice Thickness	0.5mm
Average Number	1
NEX	1
RF Pulse	Sinc7H, sinc3

The co-cultured tumor spheroids were removed from the incubator. Agar with DMEM was heated and 50ul transferred into an Eppendorf tube. The tumor spheroid was injected beneath the surface when agar was still jelly followed by cooling down for an hour.

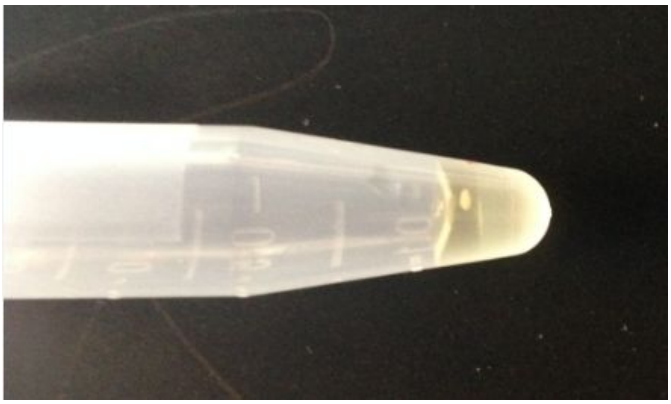

Fig 40. **Tumor Spheroid Cells in Agar.**

Using T2 weighted imaging, the tumor spheroid was visible as a clear bright spot with good CNR.

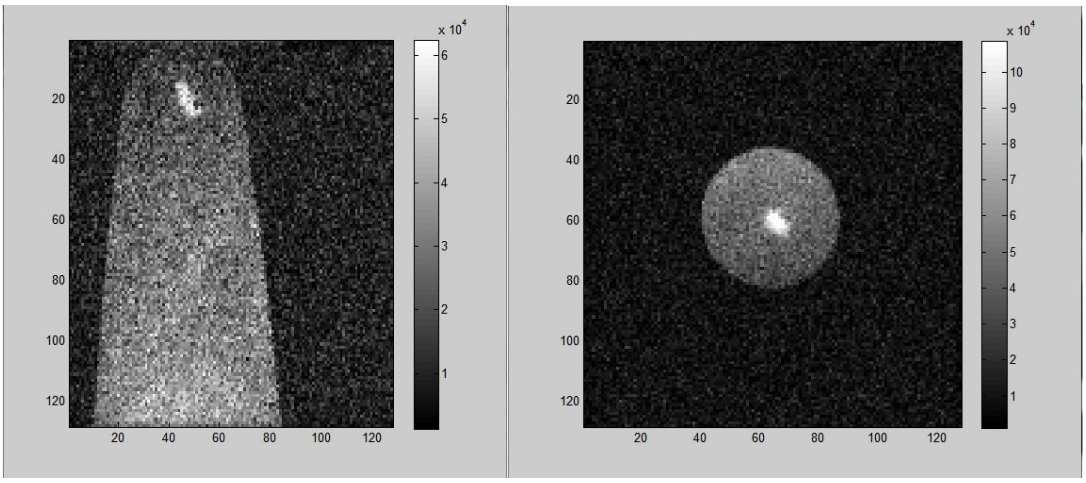

Fig 41. **T2 Axial Scanning and Coronal Scanning.**

6.5 PISTOL Imaging of Siloxane

As discussed in section 3.1, PISTOL sequence is used to specifically image siloxane particles and eliminate the influence of water and fat resonance, which will provide us a better selective imaging. Since this new coil had been successful in mesoscopy, next task was PISTOL imaging of polydimethylsiloxane (PDMS) in vitro.

In my experiments, PDMS with a molecular weight of 410 g/mol was utilized in place of hexamethyldisiloxane (HMDSO). HMDSO nanoemulsions were found to undergo phase separation after synthesis, whereas nanoemulsions with PDMS did not separate and remained stable over longer periods of time. In previous studies by our group, PDMS has also been shown as an oxygen reporter molecule (pO_2), and can be combined with a fluorescent component to create dual-modaility (MRI/Fluorescence), dual-functionality (oximetry/detection) nanoprobes for cellular and molecular imaging.

First trial was performed using a 20ul PDMS bubble in agar. Agar with DMEM was heated above melting point and 50ul was transferred into and Eppendorf tube to cool down for an hour. Injection was made through Hamilton needle (Hamilton; Reno, NV, USA). Even though compared to the size of spheroid the 20ul volume was quite large, it was essential test for my coil's performance for PISTOL imaging.

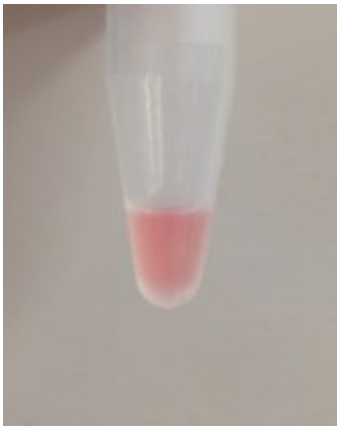

Fig 42. **Sample of Agar/PDMS Bubble.** Within 20ul PDMS bubble suspend in Agar substrate.

Using the PISTOL sequence developed by Dr. Vikram Kodibagkar and implemented on the Bruker system by Rohini Shankar, frequency-selective signal detection of the PDMS was achieved. The experiment ran under room temperature (23℃).

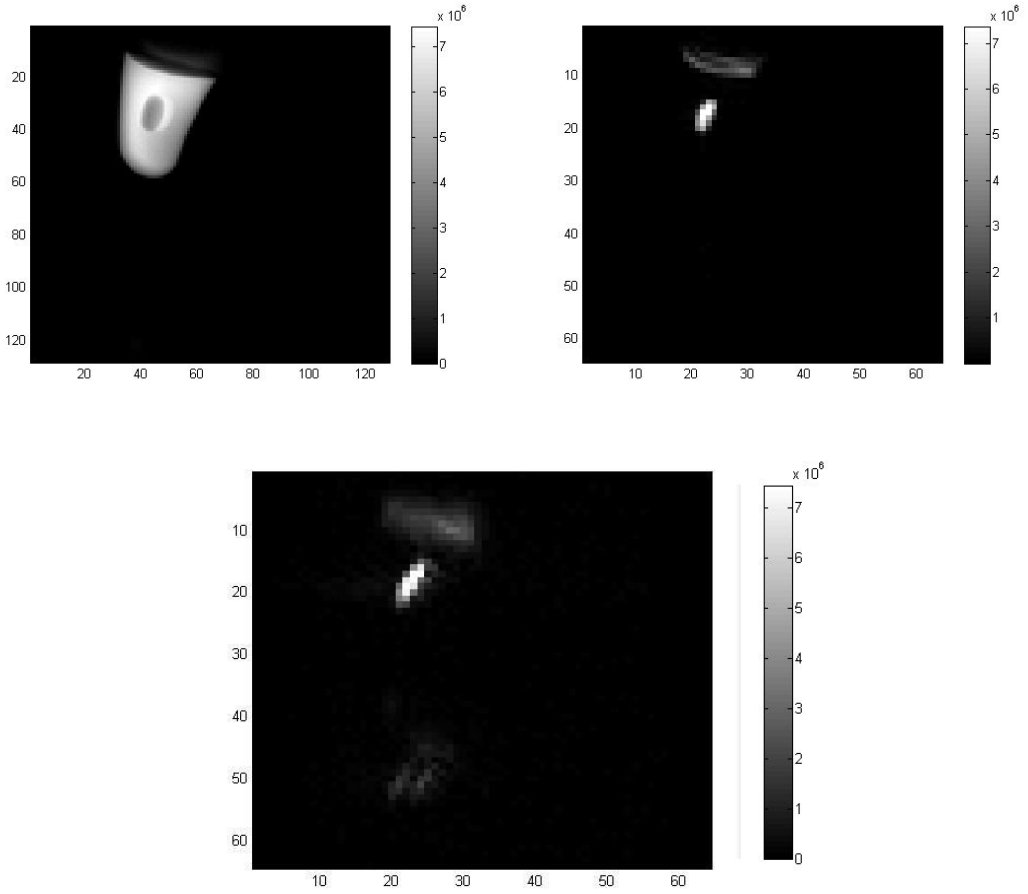

Fig 43. **T2 Weighted, HMDSO MSME and PISTOL Images of 20ul PDMS Bubble.** Reference T2 image (left), shimmed HMDSO MSME (right) and following PISTOL (down) scanning. The PISTOL image shows SNR of 220.

In PISTOL image, PDMS bubble was brightened in middle position and the "EPI ghost" of whole PDMS sample appeared in bottom displaced by half FOV as expected. Our Matlab code permitted ROI selection to exclude the ghost. Both T1 map and partial pressure of oxygen map are shown below..

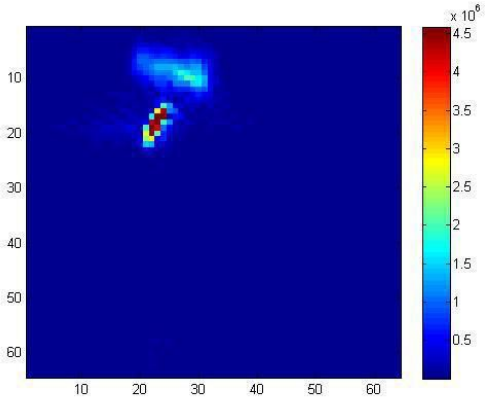

Fig 44. **ROI Selected Colorful PISTOL Image of 20ul PDMS Bubble**

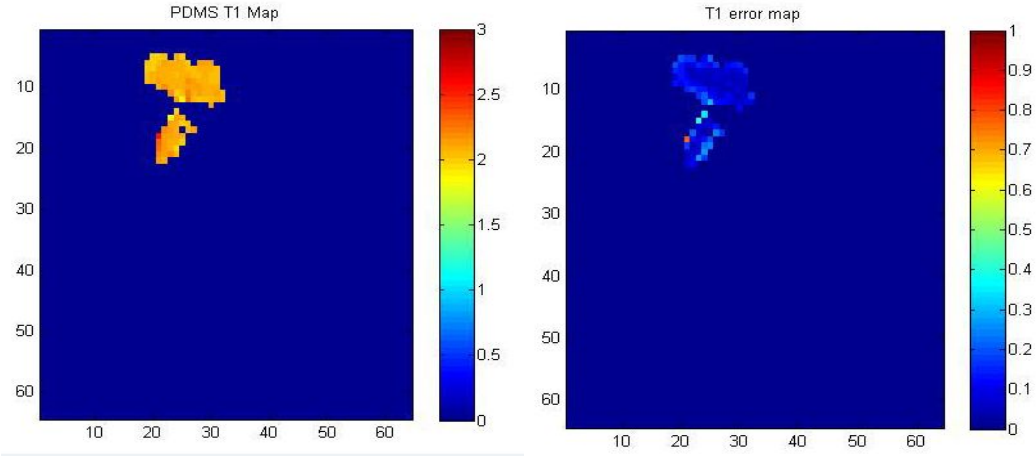

Fig 45. **T1 Map and Error Map of 20ul PDMS Bubble**

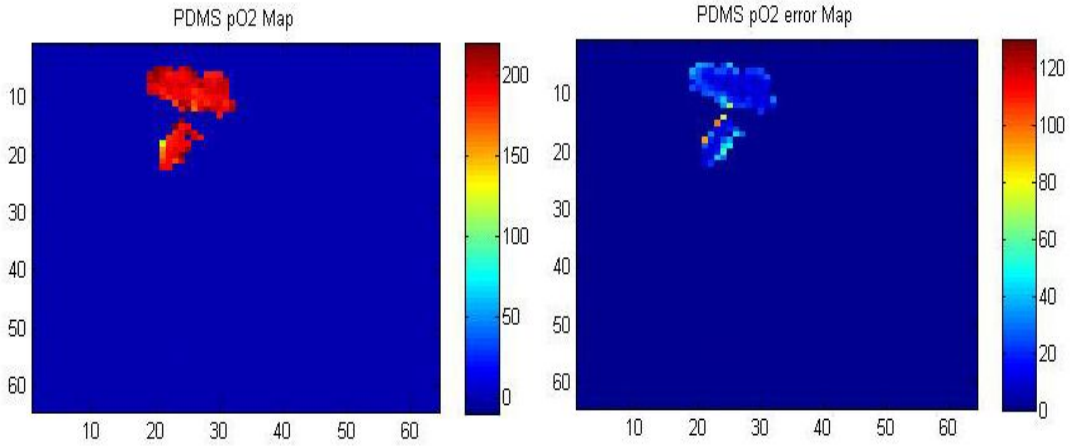

Fig 46**. pO_2 Map and Error Map of 20ul PDMS Bubble.**

Measurement was carried out under the ambient conditions. The mean pO_2 value (180 ± 23 torr) is close to the value we expect in ambient air. i.e. partial pressure of oxygen (pO_2) of 160 Torr. The deviation may result from differences in temperature of this experiment from the calibration experiment performed by our group in the past.

Next the above experiment was repeated using a 1ul PDMS sample made as described before.

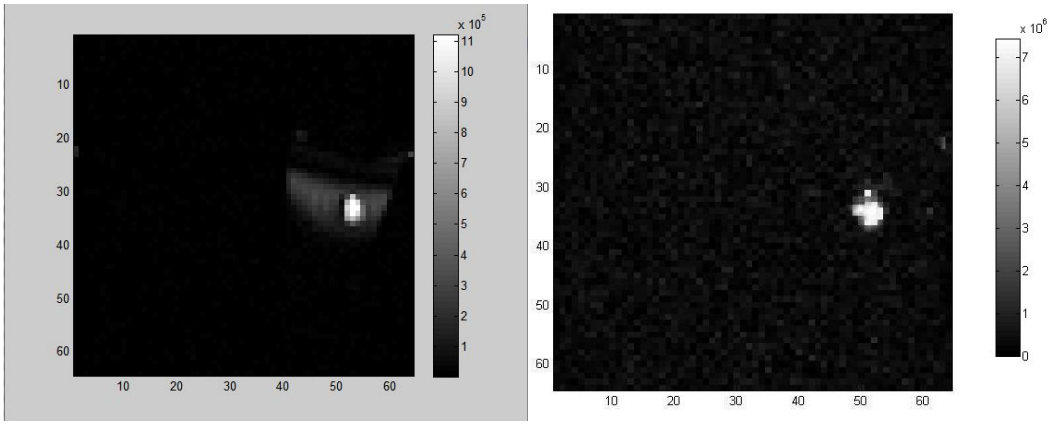

Fig 47. **T2 Weighted and HMDSO MSME Images in 1ul PDMS Trail.**

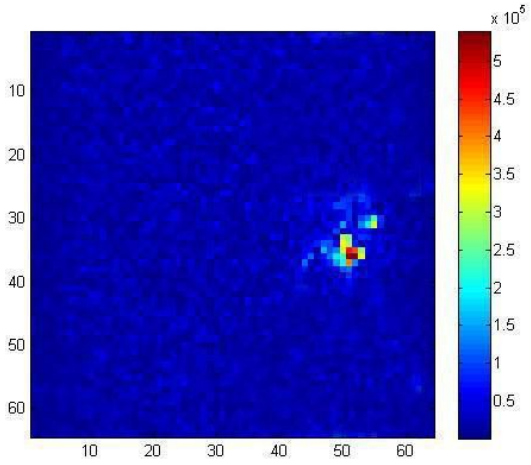

Fig 48. **PISTOL Image of 1ul PDMS Bubble**

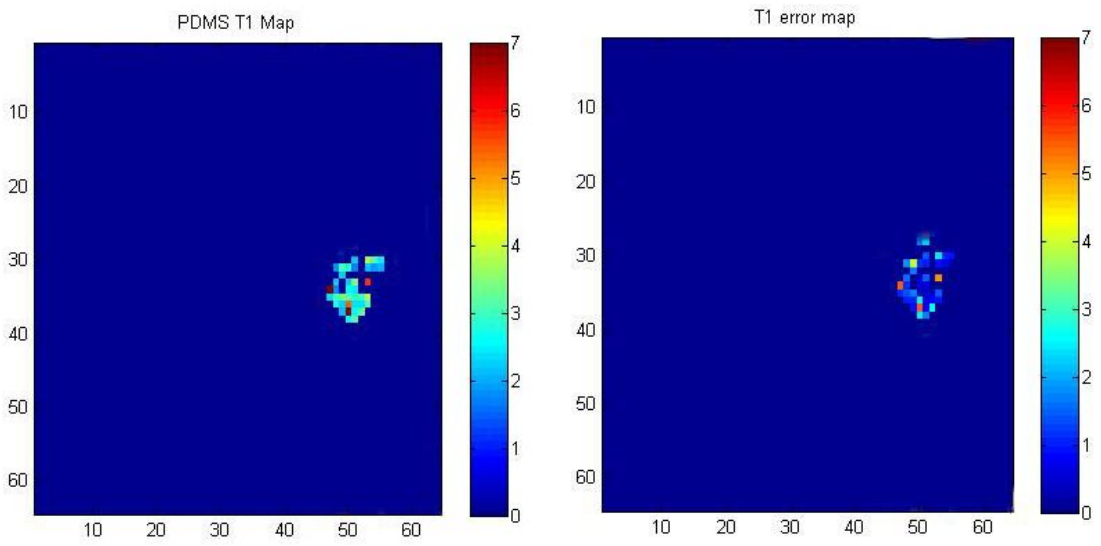

Fig 49. **T1 Map and Error Map of 1ul PDMS Bubble**

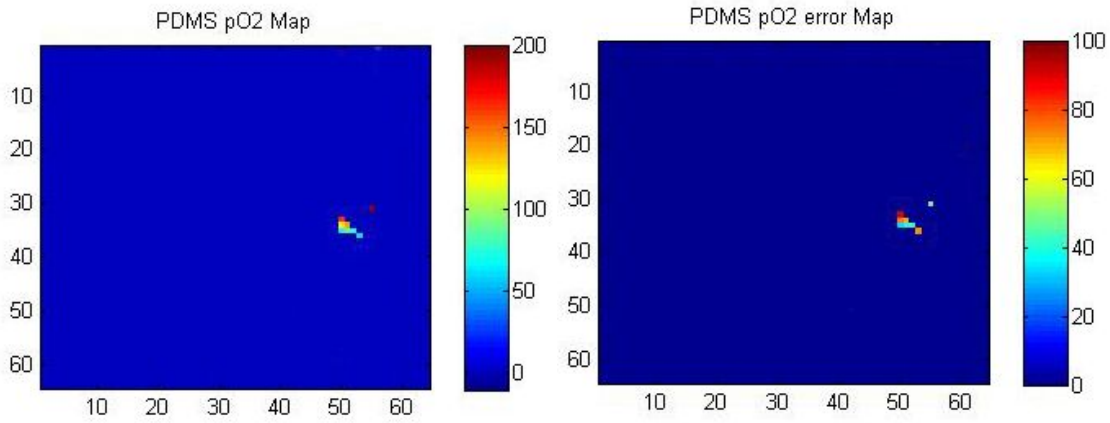

Fig 50. **pO_2 Map and Error Map of 1ul PDMS Bubble.**

Obviously, the drastic decrease of PDMS volume led to a drop of SNR (56.4) because the intensity of useful signal from PDMS drop 20 times while the background noise remained. In total, 3 trials were run and two of them failed to register on the siloxane selective T2 imaging due to low intensity of signal. This may have been due to

the total amount of PDMS was too low and the unintentional spread of the injected siloxane. However, the SNR and CNR of successful sample taken were good which confirmed new coil be able to image larger tumor spheroid cells. According to the fluorescence imaging before, I assume a spheroid's radius to be 450um, which leads to a volume of spheroid V=4(pi*r^3)/3 ~ 0.3ul. Assuming the unrealistic case of 100% labeling, the maximum possible volume of PDMS is 0.3ul. The 1ul volume of PDMS does not represent the real tumor spheroid volume, but at 0.3 ul, we would expect a, SNR of ~ 6 from above in absence of signal averaging. The actual conditions likely call for detection at near an order of magnitude less because it is impossible to label cells completely. A better estimation would be to consider the cells 10 percent labeled resulting in a maximum of 0.3 μL of siloxane injected. It is more likely to give a maximum siloxane volume somewhere within the window of 0.03 μL. With this in mind, identifying ways to increase siloxane detection sensitivity even further is needed.

6.6 PISTOL Imaging of Siloxane Labeled Spheroid Tumor

Tumor spheroids were labeled in a total of 2, 4 and 6 hours after structural formation as described in Chapter 6.2. Spheroids were immersed in agarose gel within 2.0 mL Eppendorf tubes to minimize susceptibility. Fluorescence imaging was performed to evaluate the degree of labeling by Xenogen fluorescence system available at BNI.

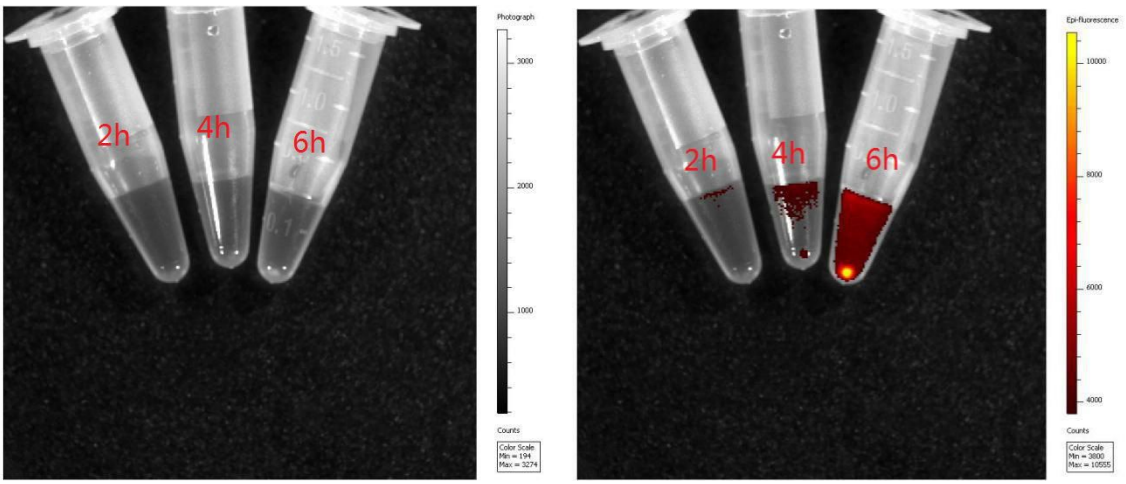

Fig 51. **Overlay Fluorescence Images of Labeled Spheroid Tumor Cells.** Reference (left) and fluorescence imaging of 2, 4 and 6 hours labeling (from left to right) . Fluorescence image in 6 hours: excitation – 500 nm, emission – 580 nm

The spheroids labeled for 6 hours showed strongest intensity which implied high uptake of emulsion. Therefore 6 hours labeling was employed in next scanning. Following figures display the ability to view labeled spheroids *in vitro*. It is encouraging to see localized signal from where the spheroid appears to be on the T_2 anatomical image and correlating PISTOL imaging. Using a long echo time, signal from water decreases while siloxane signal remains bright per its long T_2.

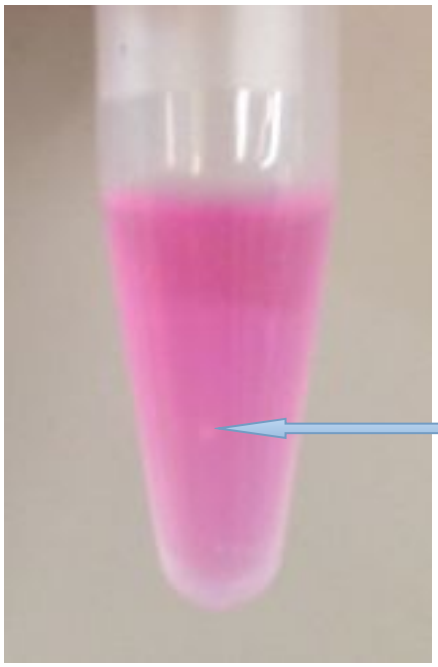

Fig 52. **Labeled Spheroid Tumor Cells Sample.** Spheroid suspended in pure Agar substrate

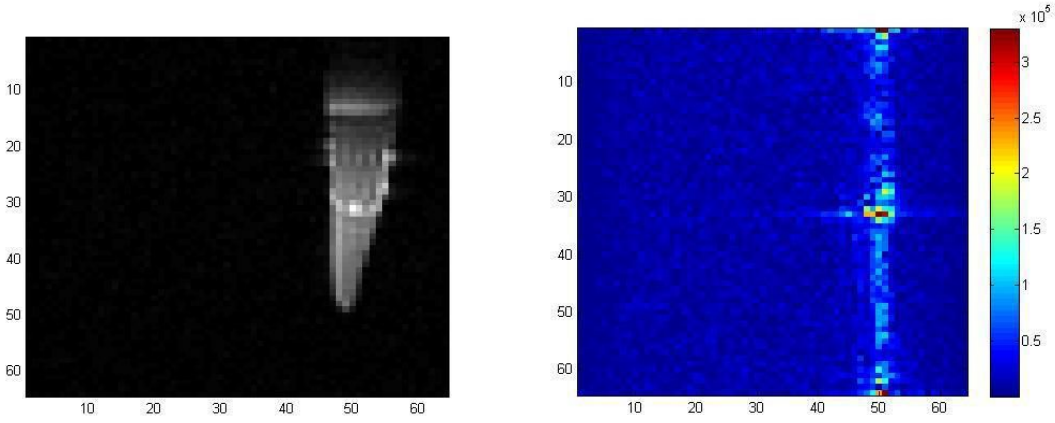

Fig 53. **PISTOL Imaging of 6 Hours Labeled Spheroid Tumor Cells.** Reference T2 weighted (left) and PISTOL imaging (right).

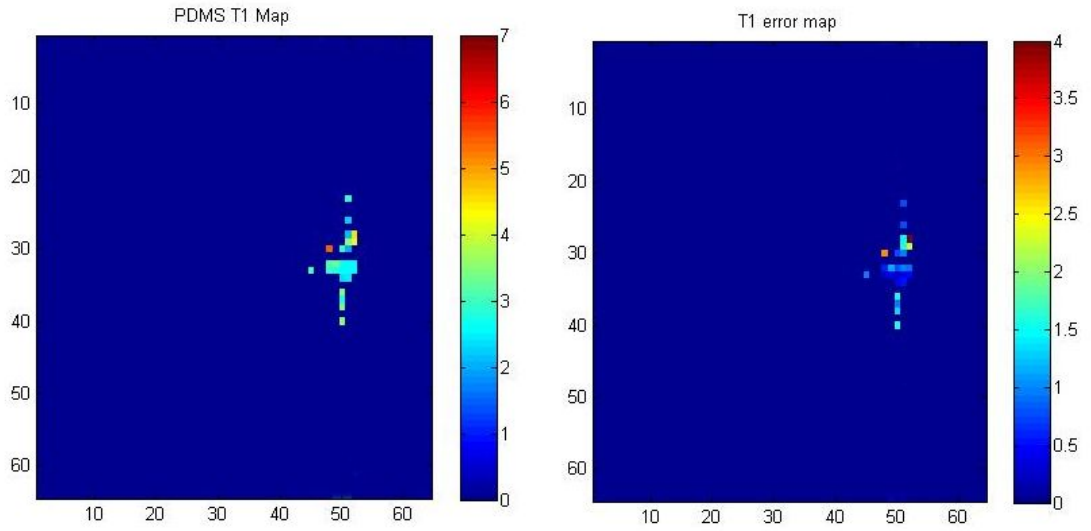

Fig 54. **Spheroid's T1 Map and Error Map.**

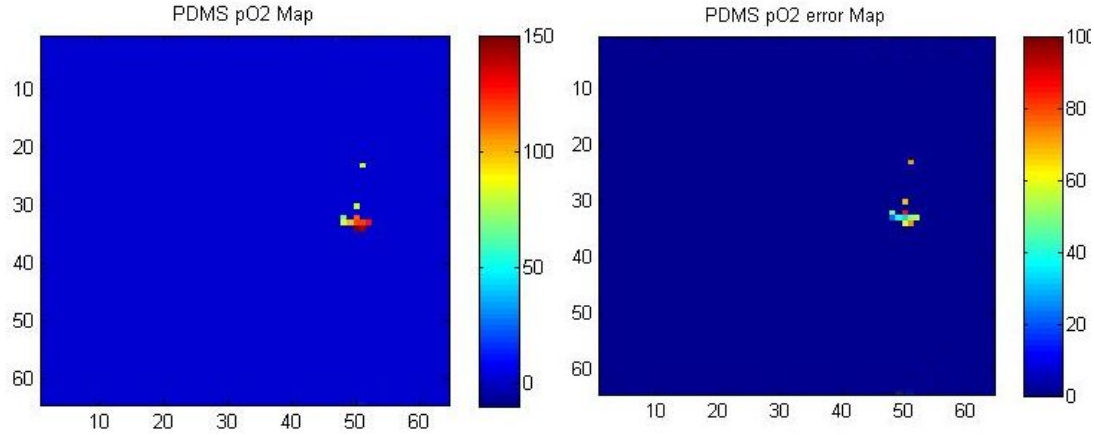

Fig 55. **Spheroid pO_2 Map and Error Map.** Spheroid ROI has pO_2=127±20 torr

6 hours long incubation time enabled a higher payload of nanoemulsion within the cells and gave a signal increase. Successful PISTOL imaging followed by pO_2 calculation showed the ability of my coil to detect siloxane resonance from labelled tumor spheroids and perform functional measurements at mesoscale.

7 DISCUSSION AND CONCLUSION

In this work, a novel RF coil for imaging of mesoscale samples has been built and tested. In this thesis, I have discussed the theory and the steps of designing and manufacture of circuit and coil unit. The design and the development of interface circuit and the coil were carried out individually. The development of interface circuit and the specific coil comprised of simulating the design, creating a compact layout and comparing with commercial one. Further improvements in the design could include a bridge circuit and integrated preamplifier which will lead to even higher sensitivity.

From an imaging point, higher field strength B_0 will potentially result in stronger signal. A stronger magnet creates a larger discrepancy between high energy and low energy nuclear spins creating a larger bulk magnetization when a sample is exposed to an external magnetic field [13]. Thus stronger magnetic field should works for detection the sample smaller than 1ul volume. Additionally, signal to noise ratio increases at higher fields, which means less noise and signal will be easy to check. Unfortunately, most clinical imaging is done at 1.5 and 3T fields at lower strength than the Bruker 7T so this maybe not feasible. Thus it becomes a matter of parameter optimization for coil design. All of experiments performed here were in vitro studies, however, in vivo, more issues need to be considered.

First, the surface coil may be more appropriate because it has better SNR and smaller FOV. In vivo test, mini surface coil may work, but sacrifice homogeneity to trade for good SNR and sensitivity. Besides, the distance between coil and tumor is another issue but not a big problem cause the injection of cells is controllable.

Secondly, the siloxane contrast agents are susceptible to artifacts, and acquisition parameters must be optimized. Chemical shift edge artifacts [15, 16] can occur, but the more applicable concerns involve the susceptibility artifact and background signal elimination. These concerns can be addressed with increased attempts at boosting local field homogeneity (shimming) and suppression techniques. Overcoming these issues is plausible, but requires attention to optimizing acquisition conditions during scans.

REFERENCES

1. Jin, Jianming. Electromagnetic Analysis and Design in Magnetic Resonance Imaging. Boca Raton, Fl: CRC Press LLC; 1989.

2. Liang, Z.; Lauterbur, P. Principles of Magnetic Resonance Imaging: A Signal Processing Perspective. Wiley-IEEE Press; 2000.

3. Mihaela Lupu, Andre Briguet, Joel Mispelter. NMR Probeheads: For Biophysical and Biomedical Experiments. Imperial College Press; 2006

4. C.E. Hayes, W.A. Edelstein, J.F. Schenck. Radio Frequency Resonators.In Magnetic Resonance Imaging. Philadelphia, 1988

5. Hood, Maureen N., et al. "Chemical shift: the artifact and clinical tool revisited." Radiographics 19.2 (1999): 357-371.

6. Menon JU, Gulaka PK, McKay MA, Geethanath S, Liu L, Kodibagkar VD. Dual-Modality, Dual-Functional Nanoprobes for Cellular and Molecular Imaging. Theranostics 2012; 2(12):1199-1207. doi:10.7150/thno.4812.

7. Kodibagkar, Vikram D., et al. "Proton imaging of siloxanes to map tissue oxygenation levels (PISTOL): a tool for quantitative tissue oximetry." NMR in biomedicine 21.8 (2008): 899-907

8. Ruiz-Cabello Jesús, et al. "Fluorine (19F) MRS and MRI in biomedicine.", NMR in Biomedicine 24.2 (2011): 114-129.

9. Tsien, Roger Y., and Alan Waggoner. "Fluorophores for confocal microscopy." Handbook of biological confocal microscopy. Springer US, 1995. 267-279.

10. Kuperman, Vadim.Magnetic Resonance Imaging: Physical Principles and Applications. San Diego: Academic Press, 2000.

11. ISO 12232: 1997 Photography - Electronic Still Picture Cameras - Determining ISO Speed here

12. Murphey-Boesh, J., and Koresky, A.P., 1983

13. Caravan, Peter. "Strategies for increasing the sensitivity of gadolinium based MRI contrast agents." Chemical Society Reviews 35.6 (2006): 512-523.

14. Babcock, Evelyn E., et al. "Edge artifacts in MR images: chemical shift effect." Journal of computer assisted tomography 9.2 (1985): 252-257.

15. Dwyer, Andrew J., Richard H. Knop, and D. I. Hoult. "Frequency shift artifacts in MR imaging." Journal of computer assisted tomography 9.1 (1985): 16-18.

16. Mahdi Jafari, Seid, Yinghe He, and Bhesh Bhandari. "Nano-emulsion production by sonication and microfluidization—a comparison." International Journal of Food Properties 9.3 (2006): 475-485.

APPENDIX A

MATLAB CODE

%Matlab code of value determination:

```
% all diameter 1.1cm    radius of copper wire 1mm
% L=13e-9H              measured

clc
clear all
r=0.2;                  % resistance of copper coil, ohms
w=2*pi*3*10^8;              % center freq set 300MHz, rads/s
L=13*10^(-9);           % inductance of coil, H
Q=L*w/r                 % quanlity factor
B=r*(1+Q^2);
A=(B/50-1)^(1/2);
CT=10^(12)*(Q+A)/(B*w)      %unit pF
CM=10^(12)/(w*50*A)         %unit pF
```

%Matlab code of voltage phase plot:

```
clc
clear all

f=3e8;   %frequency
```

```
w=2*pi*f;    % rad/s
L=13e-9;     % coil inductance
R=0.2;
ct=23e-12;    % tuning
cm1=2.7e-12;   % fix matching capacitor
cm2=2.82e-12;  % adjustable matching capacitor

Zl=i*w*L;
Zct=1/(i*w*ct);
Zbing=1/(1/(Zl+R)+1/Zct)
Zcm1=1/(i*w*cm1)
Zcm2=1/(i*w*cm2)

V=1;

Ztotal=Zcm1+Zcm2+Zbing;
I=V/Ztotal;

VA=I*(Zbing+Zcm2)
VB=I*Zcm2
AngleA=angle(VA);
AngleB=angle(VB);
```

%Matlab code for plot :

```
clc
clear all
x = [];
h = [];
r = [];
plot(x,h, 'ro-')
hold
plot(x,r, 'go-')

title('Comparison Agar T1 a/s')
xlabel('TR (ms)')
ylabel('SNR')
```